https://novapublishers.com/shop/an-essential-guide-to-electrodynamics/

An Essential Guide to Electrodynamics

Editor: Norma Brewer

ISBN: 978-1-53615-705-5Categories: Particle Physics, Physics and Astronomy, Physics Research and TechnologyTags: particle physics, 9781536157161, 9781536157055

Publication Date: July 2019
Status: In Production
282 pages

Nova Science Publishers, Inc.
415 Oser Avenue, Suite N
Hauppauge, NY, 11788 USA
Tel: 1-631-231-7269
Fax: 1-631-231-8175
Email: a.vranick@novapublishers.com
Web: www.novapublishers.com

Chapter

RADIATION OF ELECTROMAGNETIC WAVES INDUCED BY ELECTRON BEAM PASSAGE OVER ARTIFICIAL MATERIAL PERIODIC INTERFACES

Yuriy Sirenko[1,2*], Petro Melezhik[1], Anatoliy Poyedinchuk[1], Seil Sautbekov[3], Alexandr Shmat'ko[4], Kostyantyn Sirenko[1], Alexey Vertiy[1], and Nataliya Yashina[1]

[1]Department of Diffraction Theory and Diffraction Electronics, *O.Ya. Usikov* Institute for Radiophysics and Electronics, Kharkiv, Ukraine

[2]Department of Applied Mathematics, *V.N. Karazin* Kharkiv National University, Kharkiv, Ukraine

[3]Department of Physics and Technology, *Al-Farabi* Kazakh National University, Almaty, Republic of Kazakhstan

[4]Department of Radiophysics, Biomedical Electronics and Computer Systems, *V.N. Karazin* Kharkiv National University, Kharkiv, Ukraine

ABSTRACT

The chapter is focused at accurate and profound investigation, interpretation and explanation of resonant and anomalous phenomena in radiated electromagnetic field that arises due to the passage of charged particles beams

*Corresponding Author Email: yks2002sky@gmail.com

over arbitrary shaped periodic interface of natural or artificial material including smart and metamaterials. Reliability of the results is assured by the fact that the study is based on rigorous accurate solutions to electromagnetic boundary and initial boundary value problems and corresponding robust numerical algorithms.

Two types of structures are considered in theory: (i) infinite arbitrary profiled periodic interfaces of conventional or artificial materials with a priori given dispersion law, their consideration is based on frequency domain (FD) methods of analytical regularization; and (ii) infinite structures constructed of periodic arrays of various materials, their consideration is based on solutions to the corresponding electrodynamic problems, which are developed with a help of the method of exact absorbing conditions (EAC) enabling the consideration of the problems both in time domain (TD) and FD.

Keywords: analytical regularization method, method of exact absorbing conditions, density-modulated electron flow, periodic interface, artificial materials, Smith-Purcell and Vavilov-Cherenkov radiation phenomena

INTRODUCTION

A plane, density-modulated electron beam, moving at a constant speed over an infinite one-dimensional periodic grating, generates homogeneous plane electromagnetic waves in the environment space. The number of waves, their wavelength and direction of propagation are determined by the speed of the electron beam, its period of modulation, and by the length of the period of grating. The same beam moving at a constant speed in a medium, where the speed of light is less than the speed of charged particles, generates in it two homogeneous plane electromagnetic waves, diverging from the direction of flow. The length of these waves and the direction of their propagation are determined by the period of beam modulation, the ratio of its velocity to the speed of light in the medium, and by the sign of refractive index of the medium. The field of plane waves propagating above or below the grating or in a sufficiently optically dense medium is generated by the field of the charged particles flow.

That may serve as a concise representation of the well-known effects of Smith-Purcell and Vavilov-Cherenkov radiation [1–5]. Discovered in the first half of the 20th century, they are still of a great interest, and quite often are considered in various kinds of basic and applied research. Adequate modeling of these effects, the analysis of physical features observed in their implementation at periodic interfaces between media (conventional and artificial with non-standard properties) is the main topic of this work.

In electromagnetic modeling, the field of a plane, density-modulated electron flow is identified with the field of an inhomogeneous plane wave arriving at an infinite periodic grating, or with the field of a surface (slow) wave of a dielectric waveguide located near a finite periodic structure. Within the frames of these models, only the wave analogs of the Smith-Purcell and Vavilov-Cherenkov effects are simulated. Namely, the models describe the diffraction effects of the classical grating theory and surface-to-spatial mode conversion effects: an inhomogeneous plane wave or a surface wave of an open guiding structure, whose exponentially decaying part sweeps the surface of the grating or an interface of sufficiently optically dense medium, creates in this medium or in the radiation zones of a periodic structure a wave that can propagate (if there is no attenuation) infinitely far [2,6–12]. The differences in the adequacy of the corresponding models are mainly due to the fact that the first of them implements the so-called 'approximation of a given current' or 'approximation of a given field' approach when the amplitude of an inhomogeneous plane wave, which gives energy to outgoing homogeneous plane waves, remains constant along infinite interaction space with periodic structure. The model of the system 'dielectric waveguide – finite grating' is free from this drawback. But it is important, that together they can effectively and accurately solve all the theoretical and practical problems related to the study and practical application of the Smith-Purcell and Vavilov-Cherenkov effects, and their wave analogs. In the theoretical part of this chapter, we consider only those models that implement the approximation of a given field.

For periodic structures made of conventional materials, such effects (diffraction radiation effects) have been consistently and thoroughly, theoretically and experimentally studied in the last three decades of the 20th century in *O.Ya. Usikov* Institute for Radiophysics and Electronics, Kharkiv, Ukraine (IRE NASU) in the department headed by academician Viktor Shestopalov. In numerical simulations, the models of the method of analytical regularization [8,13–19] implementing the approximation of a given current have been used, and the radiation field of an infinite one-dimensionally periodic grating placed in the field of an inhomogeneous plane wave was studied. The practical outputs resulted in the creation of the diffraction radiation generators – stable, coherent sources of the millimeter range electromagnetic waves, operating on the Smith-Purcell effect [2,20,21], in the construction of planar and linear diffraction antennas [11,12,22–28], unique in their characteristics, for radar and radiometric ground, airborne and satellite-based complexes of different purpose. The method of exact absorbing conditions developed in the last two decades for solving initial-boundary problems of computational electrodynamics [11,12,29–38] allowed significant progress in the directions indicated above; a computational experiment, carried out for models

'dielectric waveguide – finite grating', now gives the same reliable results as a full-scale experiment. But much faster and, that is the most important, at a much lower costs.

The resource, not yet actively involved by neither theoreticians nor applied scientists studying and exploiting the effects of diffraction radiation when solving actual practical problems, is associated with the use of artificial and smart materials. These are materials whose properties could be adjusted and modified under the influence of external factors (temperature, light, pressure), and metamaterials whose unusual electrodynamic characteristics (band gaps, negative refraction, and so on) are due to their structure (most often periodic), but not to the properties of individual substances they composed of. The scientists aiming at a significant progress in this direction will face many different problems. In this chapter we only demonstrate the possibilities of the theoretical approaches we have developed, namely the method of analytical regularization and the method of exact absorbing conditions, and their ability to effectively solve traditional and new problems arising in the study and practical application of diffraction radiation effects.

We use SI, the International System of Units, for all physical parameters except the time t that is the product of the natural time and the velocity of light in vacuum, thus t is measured in meters. According to SI, all linear geometrical parameters (a, b etc.) are given in meters. However, this is obviously not a serious obstacle to extend the results to any other geometrically similar structures. As a rule, the dimensions in the text are omitted, and the majority of results are presented in the form of dimensionless parameters.

MODELS OF THE METHOD OF ANALYTICAL REGULARIZATION

In free space, the field $\vec{U}^i(g,k)=\left\{\vec{E}^i(g,k),\vec{H}^i(g,k)\right\}$ of a plane density modulated electron beam, whose instantaneous charge density is $\rho\delta(z-a)\exp\left[i\left((k/\beta)y-kt\right)\right]$, corresponds to the H-polarized electromagnetic field ($\partial/\partial x\equiv 0$, $E_x^i=H_y^i=H_z^i=0$) and [2,39]

$$H_x^i(g,k)=2\pi\rho\beta\exp\left\{i\left[\sqrt{k^2-(k/\beta)^2}\,|z-a|+(k/\beta)y\right]\right\}\left[|z-a|/(z-a)\right];\quad z\neq a,$$
$$E_y^i(g,k)=-(\eta_0/ik)\partial_z H_x^i(g,k),\quad E_z^i(g,k)=(\eta_0/ik)\partial_y H_x^i(g,k). \tag{1}$$

Here, $\delta(...)$ is the Dirac's δ-function; ρ and k are the amplitude and frequency of the flow modulation, and $0<\beta<1$ is its relative velocity; $\eta_0=(\mu_0/\varepsilon_0)^{1/2}$ is the free space impedance, ε_0 and μ_0 are vacuum's permittivity and permeability; $g=\{y,z\}$ is a point in space R^2; $\exp(-ikt)$ is the time factor of harmonic fields.

Let $-2\pi\rho\beta\sqrt{l}\exp\left[-ka\sqrt{(1/\beta)^2-1}\right]=1$. Then the field (1) of the electrons moving over the periodic boundary S, separating the conventional medium (vacuum) and the dispersive medium (see Figure 1a), generates in the regions $z\geq 0$ and $z\leq -b$ H-polarized field $\vec{U}^s(g,k)=\{\vec{E}^s(g,k),\vec{H}^s(g,k)\}$ with nonzero components [8,17]:

$$H_x^s(g,k)=\sum_{n=-\infty}^{\infty}\varphi_n(y)\begin{cases}R_{n1}(k)\exp(i\Gamma_n z); & z\geq 0\\ T_{n1}(k)\exp\left[-i\Gamma_n^{\varepsilon,\mu}(z+b)\right]; & z\leq -b\end{cases} \tag{2}$$

and

$$E_y^s(g,k)=-\frac{\eta_0}{ik\varepsilon(g)}\partial_z H_x^s(g,k),\quad E_z^s(g,k)=\frac{\eta_0}{ik\varepsilon(g)}\partial_y H_x^s(g,k). \tag{3}$$

Here, l and b are the period and height of grating mounts $\mathrm{S}=\{g: z=f(y), -b\leq f(y)\leq 0\}$; $k=2\pi/\lambda$, λ is the wavelength of electromagnetic waves in free space; $\varepsilon(g)$ and $\mu(g)$ ($\mathrm{Im}\,\varepsilon(g)=\mathrm{Im}\,\mu(g)=0$) are relative dielectric and magnetic permeability of wave propagation medium ($\varepsilon(g)=\mu(g)\equiv 1$ for $z>f(y)$ and $\varepsilon(g)=\varepsilon(k)$, $\mu(g)=\mu(k)$ for $z<f(y)$); $\varphi_n(y)=l^{-1/2}\exp(i\Phi_n y)$, $\Phi_n=2\pi(n+\Phi)/l$, $\mathrm{Im}\,\Phi=0$, $|\Phi|<0.5$ and $\Phi_1=k/\beta$; $\Gamma_n=\Gamma_n(\Phi)=\sqrt{k^2-\Phi_n^2}$ and $\mathrm{Re}\,\Gamma_n\geq 0$, $\mathrm{Im}\,\Gamma_n\geq 0$. Signs of the real and imaginary parts of the root $\Gamma_n^{\varepsilon,\mu}=\Gamma_n^{\varepsilon,\mu}(\Phi)=\sqrt{k^2\varepsilon(k)\mu(k)-\Phi_n^2}$ are set so that all partial components $\vec{U}_n^T(g,k): H_x(g,k)=T_{n1}(k)\exp\left[-i\Gamma_n^{\varepsilon,\mu}(z+b)\right]\varphi_n(y)$ of the field $\vec{U}^s(g,k)$ in the region $z<-b$ representing fields of outgoing plane waves,

i.e. homogeneous waves ($\mathrm{Im}\Gamma_n^{\varepsilon,\mu}=0$), transferring energy in the direction $z=-\infty$, or inhomogeneous waves ($\mathrm{Re}\Gamma_n^{\varepsilon,\mu}=0$) exponentially decaying when moving in the same direction.

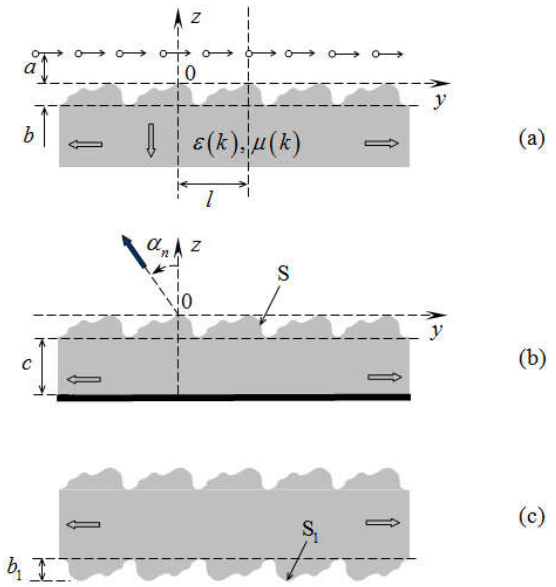

Figure 1. Structures with periodic boundary between two media: (a) half-space filled with dispersive material; (b) layer of dispersive material on metal substrate; (c) layer of dispersive material in free space.

Assuming $\Phi_1=k/\beta$, we identify the own field of the electron flow, whose exponentially decaying part sweeps the boundary S, with the field of H-polarized inhomogeneous plane wave $\vec{U}_1^i(g,k):H_x^i(g,k)=\exp(-i\Gamma_1 z)\varphi_1(y)$, $\Gamma_1=\sqrt{k^2-\Phi_1^2}=ik\sqrt{\beta^{-1}-1}$, which falls onto this boundary and generates in the reflection ($z>0$) and transition zones ($z<-b$) homogenous and inhomogeneous plane waves $\vec{U}_n^R(g,k):H_x(g,k)=R_{n1}(k)\exp(i\Gamma_n z)\varphi_n(y)$ and $\vec{U}_n^T(g,k)$. In electromagnetic grating theory these waves are called spatial harmonics of periodic structure [8,15,17]. The ones whose numbers n correspond to real propagation constants Γ_n and $\Gamma_n^{\varepsilon,\mu}$ are able to propagate infinitely far from the boundary S. In the reflection zone $z>0$, they leave boundary at the angles

$\alpha_n(k) = -\arcsin\left[\Phi_n(k)/k\right]$ that are counted anti-clockwise from the axis z. Obviously, for any fixed values k and β the number of such waves, N, is also finite $n = 0,-1,-2,...,-N+1$.

Complex amplitude coefficients $R_{n1}(k)$ and $T_{n1}(k)$ are intricate functions of the frequency k, and geometric and constitutive parameters of wave propagation media. We find them by solving numerically in the interval $0 \le y \le l$ (in the Floquet channel) the standard boundary value problem of the electrodynamic theory of gratings [8,17]

$$\begin{cases} \left[\partial_y^2 + \partial_z^2 + k^2\varepsilon(g)\mu(g)\right]H_x(g,k) = 0; \quad -b \le z \le 0 \\ H_x\left\{\partial_y H_x\right\}(l,z,k) = \exp(i2\pi\Phi)H_x\left\{\partial_y H_x\right\}(0,z,k); \quad -b \le z \le 0 \\ H_x(g,k) = \left\{\begin{matrix} H_x^i(g,k) \\ 0 \end{matrix}\right\} + \sum_{n=-\infty}^{\infty} \varphi_n(y) \begin{cases} R_{n1}(k)\exp(i\Gamma_n z); & z \ge 0 \\ T_{n1}(k)\exp\left[-i\Gamma_n^{\varepsilon,\mu}(z+b)\right]; & z \le -b \end{cases} \\ H_x(g,k) \quad \text{and} \quad \vec{E}_{tg}(q,k),\ q = \{x,y,z\} \quad \text{are continuous when crossing} \\ \quad \text{S} \quad \text{and virtual boundaries} \quad z = 0 \quad \text{and} \quad z = -b \end{cases} \tag{4}$$

relatively to the $H_x(g,k)$ component of the full field

$$\vec{U}(g,k) = \left\{\vec{E}(g,k), \vec{H}(g,k)\right\} = \begin{cases} \vec{U}_1^i(g,k) + \vec{U}^s(g,k); & z \ge 0 \\ \vec{U}^s(g,k); & z < 0 \end{cases}.$$

This problem allows to determine (in the approximation of a given current) the electromagnetic field (the field of diffraction radiation) generated by the density-modulated electron flow. In numerical solution, we use the method of analytic regularization [8,13–15,18,19], which provided most of physical and applied results of the electrodynamic theory of gratings associated with resonant and anomalous spatial-frequency and spatial-time transformations of electromagnetic fields in periodic structures [8–10,15,17,19,40].

The approach used here can be described briefly as follows [18,41]. The system of orthonormal functions $\varphi_n(y) = l^{-1/2}\exp(i\Phi_n y)$, $n = 0,\pm1,\pm2,...$ is complete in the space $\mathrm{L}_2(0,l)$ of functions with the integrable on the interval $0 \le y \le l$ module squared. This allows us to write down the conditions (4), which is related to the

continuity of the tangential field components $\vec{U}(g,k)$ on the boundary S, in the form of an infinite system of linear algebraic equations

$$\begin{cases} \sum\limits_{n=-\infty}^{\infty} F_{mn}^{+} x_n^{+} - \sum\limits_{n=-\infty}^{\infty} F_{mn}^{-} x_n^{-} = b_m^{+}; \quad m = 0, \pm 1, \pm 2, \ldots \\ \sum\limits_{n=-\infty}^{\infty} K_{mn}^{+} x_n^{+} - \varepsilon^{-1}(k) \sum\limits_{n=-\infty}^{\infty} K_{mn}^{-} x_n^{-} = b_m^{+}; \quad m = 0, \pm 1, \pm 2, \ldots \end{cases} \tag{5}$$

Here, $x_n^{+} = R_{n1} \exp(-i\Gamma_n b)$ and $x_n^{-} = T_{n1} \exp(-i\Gamma_n^{\varepsilon,\mu} b)$ are new unknowns and

$$F_{mn}^{+} = L_{m-n}^{+}(\Gamma_n), \quad F_{mn}^{-} = L_{m-n}^{-}(\Gamma_n^{\varepsilon,\mu}), \quad K_{mn}^{+} = F_{mn}^{+}\left[\frac{\Gamma_n l}{2\pi} - \frac{(m-n)\Phi_n}{\Gamma_n}\right],$$

$$K_{mn}^{-} = -F_{mn}^{-}\left[\frac{\Gamma_n^{\varepsilon,\mu} l}{2\pi} - \frac{(m-n)\Phi_n}{\Gamma_n^{\varepsilon,\mu}}\right], \quad b_m^{+} = L_m^{-}(\Gamma_1), \quad b_m^{-} = b_m^{+}\left(\frac{\Gamma_1 l}{2\pi} - \frac{m\Phi_1}{\Gamma_1}\right),$$

$$L_n^{+}(q) = \frac{1}{l}\int_0^l \mathrm{e}^{i\left[q(f(y)+b) - \frac{2\pi n}{l} y\right]} dy, \quad L_n^{-}(q) = \frac{1}{l}\int_0^l \mathrm{e}^{-i\left[qf(y) + \frac{2\pi n}{l} y\right]} dy.$$

The conversion to finite-dimensional analogues in (5) leads to ill-conditioned systems of equations, so the problem needs regularization. We begin the corresponding procedure by introducing a periodic function $\overline{f}(\overline{y}) = -f(\overline{y}l/2\pi)b^{-1}$. Assume also that the function $\overline{f}(\overline{y})$ is twice continuously differentiable. Suppose that in a finite number of points $\overline{y}_s^{+}$, $s = 1, 2, \ldots, S^{+}$ and $\overline{y}_s^{-}$, $s = 1, 2, \ldots, S^{-}$ in a period $0 \le \overline{y} \le 2\pi$, this function satisfies the following conditions:

$$\overline{f}(\overline{y}_s^{+}) = 0, \quad d_{\overline{y}}\overline{f}(\overline{y}_s^{+}) = 0, \quad d_{\overline{y}}^2\overline{f}(\overline{y}_s^{+}) > 0,$$
$$\overline{f}(\overline{y}_s^{-}) = 1, \quad d_{\overline{y}}\overline{f}(\overline{y}_s^{-}) = 0, \quad d_{\overline{y}}^2\overline{f}(\overline{y}_s^{-}) < 0.$$

Under such assumptions, we can obtain the following asymptotic estimates for the matrix elements of the system (5):

$$F_{mn}^{\pm} \approx \sum_{s=1}^{S^{\pm}} \frac{\exp\left[-i(m-n)\bar{y}_s^{\pm}\right]\exp\left[-(m-n)^2/2b\left|\Phi_n d_{\bar{y}}^2 \bar{f}\left(\bar{y}_s^{\pm}\right)\right|\right]}{\sqrt{2\pi b\left|\Phi_n d_{\bar{y}}^2 \bar{f}\left(\bar{y}_s^{\pm}\right)\right|}},$$
$$K_{mn}^{\pm} \approx \mp F_{mn}^{\pm} \frac{i2\pi mn}{l|\Phi_n|}; \quad |n|,|m| \to \infty. \tag{6}$$

From (6), in particular, it follows that (5) is an operator equation of the first kind, and this is precisely what makes impossible the application of the truncation method to solve it numerically. Using representations (6), we introduce matrix operators

$$J^{\pm} = \left\{ \delta_n^m \sqrt{\tilde{\Phi}_n 2\pi b/l} \left[\sum_{s=1}^{S^{\pm}} 1 \Big/ \sqrt{d_{\bar{y}}^2 \bar{f}\left(\bar{y}_s^{\pm}\right)} \right]^{-1} \right\}_{m,n=-\infty}^{\infty}, \quad M = \left\{ \delta_n^m \tau_n \right\}_{m,n=-\infty}^{\infty}, \tag{7}$$

and new unknowns $y^{\pm} = \left\{ y_n^{\pm} \right\}$ such that $x^{\pm} = \left\{ x_n^{\pm} \right\}_{n=-\infty}^{\infty} = J^{\pm} y^{\pm}$. Here, δ_n^m is the Kronecker symbol, $\tau_0 = 1$, $\tau_{n\neq 0} = \left(i|n|\right)^{-1}$, $\tilde{\Phi}_n = n + \Phi_1 l/2\pi$. Now we are able to carry out the right-side regularization of the system (5):

$$\begin{cases} F^+ J^+ y^+ - F^- J^- y^- = b^+ \\ K^+ J^+ y^+ - \varepsilon^{-1}(k) F^- K^- y^- = b^- \end{cases}; \quad F^{\pm} = \left\{ F_{mn}^{\pm} \right\}_{m,n=-\infty}^{\infty}, \quad K^{\pm} = \left\{ K_{mn}^{\pm} \right\}_{m,n=-\infty}^{\infty}. \tag{8}$$

Applying the operator M to the second equation of system (8), we perform the left-side regularization of the problem. After several simple transformations, we arrive at the system of operator equations

$$\begin{cases} \varepsilon(k)\left[1+\varepsilon(k)\right]^{-1} y^+ + P^+ y^+ + P^- y^- = a^+ \\ \varepsilon(k)\left[1+\varepsilon(k)\right]^{-1} y^- + Q^+ y^+ + Q^- y^- = a^- \end{cases}, \tag{9}$$

equivalent to (5). Here,

$$P^+ = \left[\varepsilon^{-1}(k) F^+ + MK^+\right] J^+, \quad P^- = -\varepsilon^{-1}(k)\left[F^- + MK^-\right] J^-,$$
$$Q^+ = \left[MK^+ - F^+\right] J^+, \quad Q^- = \left[F^- - \varepsilon^{-1}(k) MK^-\right] J^-,$$

$a^+ = \varepsilon^{-1}(k)b^+ + Mb^-$, $a^- = Mb^- - b^+$. Estimates (6) allow us to prove the compactness of operators $P^{\pm}$ and $Q^{\pm}$ in the space l_2 of infinite sequences $a = \{a_n\}_{n=-\infty}^{\infty}$ such that $\sum_n |a_n|^2 < \infty$. This means that the original problem (4) is reduced to the system of operator equations of the second kind (9) (to a system of Fredholm operator equations), which numerical solution can be obtained by the truncation method converging in the norm of the space l_2. The regularization of problem (4) is completed. Let us now analyze the most general properties of its solution $\vec{U}(g,k)$.

The Pointing's complex power theorem for field $\vec{U}(g,k)$ in the volume $[0 \le x \le 1] \times [0 \le y \le l] \times [-b \le z \le 0]$ implies the fundamental relation

$$\sum_{n=-\infty}^{\infty} \left[|R_{n1}|^2 \operatorname{Re}\Gamma_n + |T_{n1}|^2 \operatorname{Re}\Gamma_n^{\varepsilon,\mu} \varepsilon^{-1}(k) \right] (\operatorname{Im}\Gamma_1)^{-1} = 2 \operatorname{Im} R_{11}. \qquad (10)$$

This relation determines all energy characteristics of the diffraction radiation processes considered in the approximation of a given current [8,40]. The value in the left of (10) is the total electromagnetic energy $W = W^{\uparrow} + W^{\downarrow}$ radiated into the half-spaces $z \ge 0$ and $z \le -b$. The values $W_{n1}^R = |R_{n1}|^2 \operatorname{Re}\Gamma_n (\operatorname{Im}\Gamma_1)^{-1}$ and $W_{n1}^T = |T_{n1}|^2 \operatorname{Re}\Gamma_n^{\varepsilon,\mu} \varepsilon^{-1}(k) (\operatorname{Im}\Gamma_1)^{-1}$, composing $W^{\uparrow}$ and $W^{\downarrow}$, characterize the distribution of energy lost by the flow of electrons in the channels open to radiation, i.e. between harmonics of the spatial spectrum $\vec{U}_n^R(g,k)$ and $\vec{U}_n^T(g,k)$ such that $\operatorname{Re}\Gamma_n \ge 0$ and/or $\operatorname{Re}\Gamma_n^{\varepsilon,\mu} \varepsilon^{-1}(k) > 0$. The last inequality and relation $\operatorname{Re} P_y(k) = \varepsilon^{-1}(k) \sum_{n:\, \operatorname{Im}\Gamma_n^{\varepsilon,\mu}=0} |T_{n1}|^2 \Phi_n$, which is the real part of (averaged over the period l of the boundary S) component $P_y(k)$ of the complex Poynting vector $\vec{P}(k)$ of the field $\vec{U}(g,k)$ in the plane $z = -b$, allow to determine unambiguously and completely strictly the direction of phase velocity of the harmonics $\vec{U}_n^T(g,k)$ propagating in the region $z < -b$ and the energy transfer direction of this harmonic. For the conventional medium, these directions coincide and are set by the vector $\Phi_n \vec{y} - \Gamma_n^{\varepsilon,\mu} \vec{z}$, $\Gamma_n^{\varepsilon,\mu} > 0$. For the bi-negative medium $\Gamma_n^{\varepsilon,\mu} < 0$, the phase velocity is

oriented along the vector $\Phi_n\vec{y}-\Gamma_n^{\varepsilon,\mu}\vec{z}$, and the energy transfer direction is oriented along the vector $-\Phi_n\vec{y}+\Gamma_n^{\varepsilon,\mu}\vec{z}$. In a medium with only one negative constitutive parameter, the harmonics $\vec{U}_n^T(g,k)$ transferring energy in the direction $z=-\infty$ are not excited.

When $H_x^i(g,k)\equiv 0$ and k is fixed, we obtain from (4) a homogeneous (spectral) problem with nontrivial solutions $H_x(g,\bar{\Phi})$ existing for no more than a countable set of eigenvalues $\{\Phi=\bar{\Phi}\}\in \mathrm{F}$ and determining the fields of the eigen waves $\vec{U}(g,\bar{\Phi})=\{\vec{E}(g,\bar{\Phi}),\vec{H}(g,\bar{\Phi})\}$ of the periodic media interface [8,40]. If any eigen value $\bar{\Phi}$ belongs to the axis $\mathrm{Re}\,\Phi$ of the first (physical) sheet of the surface F (this is the Riemann surface onto which the solution of the problem (4) is analytically continued from the real values of the spectral parameter Φ) and $\mathrm{Im}\,\Gamma_n(\bar{\Phi})>0$, $\mathrm{Im}\,\Gamma_n^{\varepsilon,\mu}(\bar{\Phi})\varepsilon^{-1}(k)>0$ for all $n=0,\pm1,\pm2,\ldots$, then we are dealing with ordinary (or correct) surface waves propagating near a media boundary without attenuation.

Above we briefly described the main points related to the use of the analytical regularization method for analyzing the effects of diffraction radiation in the system 'flat, density-modulated electron flow – periodic boundary of a conventional medium and a dispersive medium'. Obviously, the method of generalized scattering matrices provides an accurate solution to the model boundary value problem (4) arising in the case of more complex objects placed in the field of a beam of charged particles (see Figures 1b and 1c).

INTERFACE 'VACUUM – PLASMA-LIKE MEDIUM'. NUMERICAL RESULTS

Suppose that in the problem (4), the constitutive parameters of the medium filling the half-space $z<f(y)$ are given by the relations

$$\varepsilon(k)=1-k_\varepsilon^2/k^2 \quad \text{and} \quad \mu(k)=1-k_\mu^2/k^2. \tag{11}$$

Such a medium can be called plasma-like, and the real numbers k_ε and k_μ are its characteristic frequencies. Let us also set $l=2\pi$ for all simulated here periodic

boundaries in order to simplify all analytical and numerical results in terms of dimensionless parameters that are commonly used in the theory of periodic structures. They are coordinates $\{Y,Z\}=\{2\pi y/l, 2\pi z/l\}$, time $\tau = 2\pi t/l$, and frequency $\kappa = l/\lambda = kl/2\pi$.

The characteristic feature of periodic boundaries discussed in this section is the ability to control material parameters of a medium filling the area $z < f(y)$ with the help of external influences that change the frequencies k_ε and k_μ. Among various unusual properties of such periodic boundaries swept by the field of a density-modulated electron flow, we can distinguish resonant regimes appearing in generation of plane waves propagating into the half-spaces $z > 0$ and $z < -b$, in the case when the flow velocity is close to the phase velocity an eigen surface wave of the boundary S.

For small values k and b discussed below, the periodic boundary separating usual medium (vacuum) and dispersive medium with parameters (11) is capable of supporting forward (or direct) surface waves in the frequency range [42]

$$K_2 = k_\varepsilon k_\mu \Big/ \sqrt{k_\varepsilon^2 + k_\mu^2} < k < k_\varepsilon \Big/ \sqrt{2} = K_1; \quad k_\varepsilon > k_\mu . \tag{12}$$

The eigen values $\bar{\Phi}^{\text{direct},\pm,m}$ corresponding to these waves have form

$$\frac{2\pi}{l}\left(\bar{\Phi}^{\text{direct},\pm,m} + m\right) \approx \pm\frac{k}{k_\varepsilon}\sqrt{\frac{\left(k_\varepsilon^2 - k^2\right)\left(k_\varepsilon^2 - k_\mu^2\right)}{\left(k_\varepsilon^2 - 2k^2\right)}}; \quad m = 0, \pm 1, \pm 2, \ldots$$

In the range

$$k_\varepsilon \Big/ \sqrt{2} < k < k_\varepsilon k_\mu \Big/ \sqrt{k_\varepsilon^2 + k_\mu^2}; \quad k_\varepsilon < k_\mu \tag{13}$$

the same boundary can support backward waves, which have oppositely directed phase and group velocities. For such waves

$$\frac{2\pi}{l}\left(\bar{\Phi}^{\text{back},\pm,m} + m\right) \approx \pm\frac{k}{k_\varepsilon}\sqrt{\frac{\left(k_\varepsilon^2 - k^2\right)\left(k_\mu^2 - k_\varepsilon^2\right)}{\left(2k^2 - k_\varepsilon^2\right)}}; \quad m = 0, \pm 1, \pm 2, \ldots$$

The velocity of electrons moving synchronically with surface waves is determined by the relations (synchronism conditions) $\beta = kl/2\pi\overline{\Phi}^{\text{direct},\pm,m}$ or $\beta = kl/2\pi\overline{\Phi}^{\text{back},\pm,m}$.

Vavilov-Cherenkov radiation into the lower half-space occupied by a dispersive medium (radiation of the harmonic $\vec{U}_1^T(g,k)$) is possible if the condition $\operatorname{Re}\Gamma_1^{\varepsilon,\mu}\varepsilon^{-1}(k) > 0$ holds or, equivalently, the condition $\beta^2 > \left[\varepsilon(k)\mu(k)\right]^{-1}$ holds, i.e. only in the case of a bi-negative or bi-positive (conventional environment) medium. Hence, for the dispersion law (11) we obtain the following restriction on the frequency range in which Vavilov-Cherenkov radiation can be observed:

$$k < K_0 = \sqrt{2}k_\varepsilon k_\mu \Big/ \sqrt{k_\varepsilon^2 + k_\mu^2 + \sqrt{\left(k_\varepsilon^2 - k_\mu^2\right)^2 + 4k_\varepsilon^2 k_\mu^2/\beta}}\,. \qquad (14)$$

For all β from the interval $0 < \beta < 1$, the value $K_0 < k_\varepsilon k_\mu \Big/ \sqrt{k_\varepsilon^2 + k_\mu^2}$, $K_0 \to 0$ for $\beta \to 0$ and $K_0 \to k_\varepsilon k_\mu \Big/ \sqrt{k_\varepsilon^2 + k_\mu^2}$ when $\beta \to 1$. The parameter intervals (13) and (14), which provide the possibility of existence of backward surface waves, partially overlap. The frequency band where forward surface waves can exist does not overlap the frequency interval (14).

One more special feature of the periodic boundary of the medium with parameters (11) should be discussed before proceeding to the analysis of the results of computational experiments. In [41], the existence of a finite accumulation point $\overline{k}^{\text{accum}} = k_\varepsilon/\sqrt{2}$ in the spectrum of an operator of the problem (4) corresponding to such a boundary was proved. The set of complex frequencies $k = \overline{k} \in \mathrm{K}$ corresponding to non-trivial solutions $\vec{U}(g,\overline{k}) = \left\{\vec{E}(g,\overline{k}), \vec{H}(g,\overline{k})\right\}$ of the homogeneous ($H_x^i(g,k) \equiv 0$) problem (4) is called its spectrum. Functions $\vec{U}(g,\overline{k})$ are eigen oscillations of the field of the structure, relevant to eigen frequencies $\overline{k}$; K is the Riemannian surface, which defines the natural limits of the analytic continuation of the problem (4) to the domain of complex parameter values k [8,40]. The existence of a real point of accumulation $\overline{k}^{\text{accum}}$ is manifested in the thickening of resonant peaks in the amplitude-frequency characteristics of the structure in the close vicinity of the frequency $k = \overline{k}^{\text{accum}}$.

It is extremely important in the study of diffraction radiation to determine correctly the limits of parameter variation where the given regime of electron flow field transformation into the field of waves outgoing infinitely far from the periodic interface between the media is implemented. The regime identifier $\{N^+, N^-\}$ is given by the number of harmonics N^+ and N^-, which propagate without attenuation in the reflection and transition zones of the periodic structure, and the boundaries of the domains corresponding to this regime in the plane of the variables k and β are given by the curves $\mathrm{G}_n^+ : \Gamma_n(k,\beta) = 0$ and $\mathrm{G}_n^- : \Gamma_n^{\varepsilon,\mu}(k,\beta) = 0$. Here, n are the numbers of harmonics $\vec{U}_n^R(g,k)$ and $\vec{U}_n^T(g,k)$, included in the numbers N^+ and N^-.

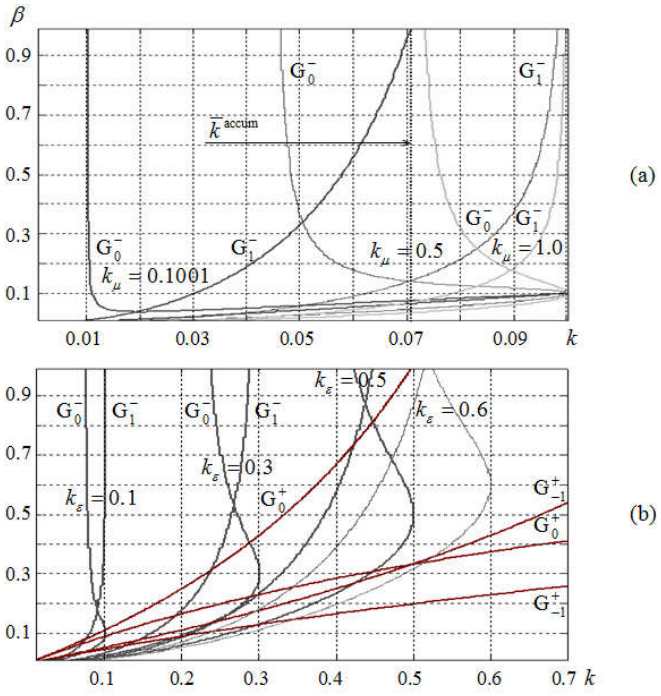

Figure 2. To the determination of the parameters variations domains where the Vavilov-Cherenkov radiation can be observed ($l = 2\pi$): (a) $k_\varepsilon = 0.1$; (b) $k_\mu = 1.0$.

In Figure 2, for the parameter values k and β from the region situated to the left from the curve G_n^-, the wave $\vec{U}_n^T(g,k)$ propagates in the structure's transition zone without attenuation. In the reflection zone, the wave $\vec{U}_n^R(g,k)$ propagates without attenuation for the parameter values k and β from the domain located between the branches of V-shaped curve G_n^+. With this in mind, we can easily determine the domains of parameter values variation for which, in the situation under consideration, Vavilov-Cherenkov radiation is implemented, and radiation of harmonics $\vec{U}_n^R(g,k)$ for all n and of harmonics $\vec{U}_n^T(g,k)$ for $n \neq 1$ (Smith-Purcell radiation) is absent. On the fragments of Figures 3, 4, and 5, all the points $\{k,\beta\}$ lying between the curves G_1^- and G_0^- (the curve G_0^- is passing to the left of G_1^-) can be attributed to these domains.

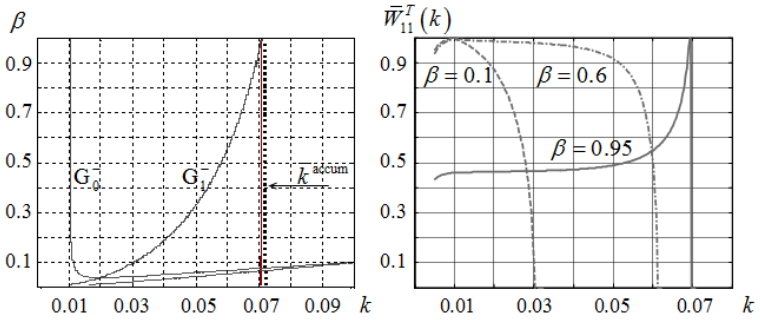

Figure 3. Efficiency of the reverse Vavilov-Cherenkov radiation (diffraction radiation on harmonic $\vec{U}_1^T(g,k)$) into dispersive medium with characteristic frequencies $k_\varepsilon = 0.1$, $k_\mu = 0.10001$ and sinusoidal boundary $z = 0.5b\left[\cos(2\pi y/l) - 1\right]$, $l = 2\pi$, $b = 0.4$.

Figure 3 shows the results of one of the computational experiments related to determining the energy characteristics $\bar{W}_{11}^T(k) = W_{11}^T(k) \Big/ \max\limits_k W_{11}^T(k)$ ($\max\limits_k W_{11}^T(k)$ is equal to 2.5288 for $\beta = 0.95$, 1.9148 for $\beta = 0.6$, and 0.3876 for $\beta = 0.2$) of the Vavilov-Cherenkov reverse radiation – the permittivity and permeability of the dispersive medium in the frequency range considered $0.01 \le k \le 0.09$ are negative. When $\beta \to 1$, the boundary G_1^- of the Vavilov-Cherenkov radiation region

approaches the straight line $k = \bar{k}^{\text{accum}} \approx 0.07$, but does not intersect it. On the curve located slightly to the left of the straight line $k = \bar{k}^{\text{accum}}$ and intersecting for large β the boundary G_1^-, one of the synchronism conditions is fulfilled. Therefore, for $\beta = 0.95$, the characteristic $\bar{W}_{11}^T(k)$ on the right fragment of Figure 3 changes much more dynamically than the similar characteristics for $\beta = 0.1$ and $\beta = 0.6$.

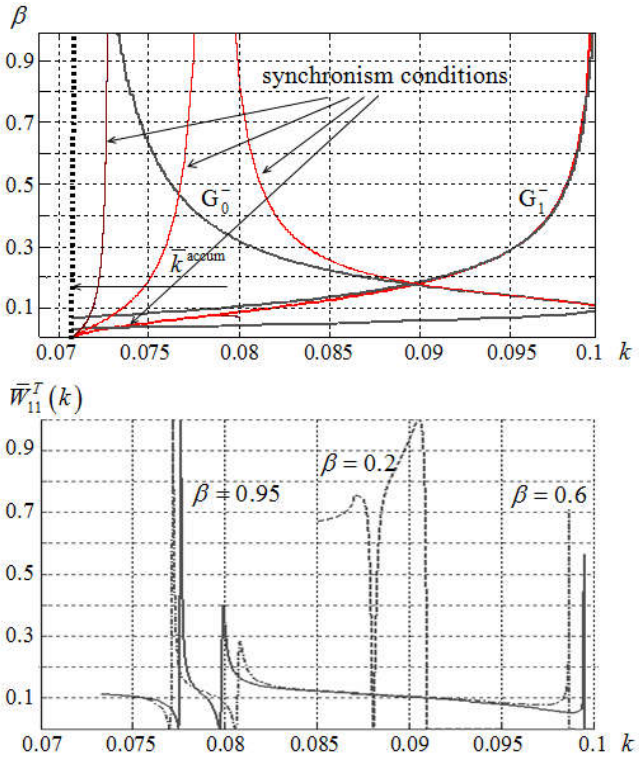

Figure 4. Same as in Figure 3, but for dispersive medium with parameters $k_\varepsilon = 0.1,\ k_\mu = 1.0$.

Figure 4 illustrates the implementation of reverse Vavilov-Cherenkov radiation for the periodic boundary of the dispersive medium with the parameters $k_\varepsilon = 0.1$ and $k_\mu = 1.0$, $-1.0 \le \varepsilon(k) \le 0$, $\mu(k) << \varepsilon(k)$ in the frequency band $0.07 \le k \le 0.1$. As the flow velocity β increases, the frequency band where these effects can be observed (the interval between the boundaries G_0^- and G_1^-) becomes

wider and can contain from two to three points $\{k,\beta\}^{\text{synchr}}$ which fulfill one of the synchronism conditions. As a result, on the curve $\bar{W}_{11}^{T}(k,\beta)$ ($\max\limits_{k} W_{11}^{T}(k)$ is equal to 0.6538 for $\beta=0.95$, 2.6676 for $\beta=0.6$, and 1.4276 for $\beta=0.2$), we observe two (for $\beta=0.2$) or even three (for $\beta=0.6$ and $\beta=0.95$) resonant peaks. The accumulation point $k=\bar{k}^{\text{accum}}\approx 0.07$ is out of the frequency band with pure Vavilov-Cherenkov radiation. Therefore, all resonant bursts of characteristics are easily predicted using the synchronism conditions and information about the approximate values of the eigen values $\bar{\Phi}^{\text{direct},\pm,m}$, $\bar{\Phi}^{\text{back},\pm,m}$.

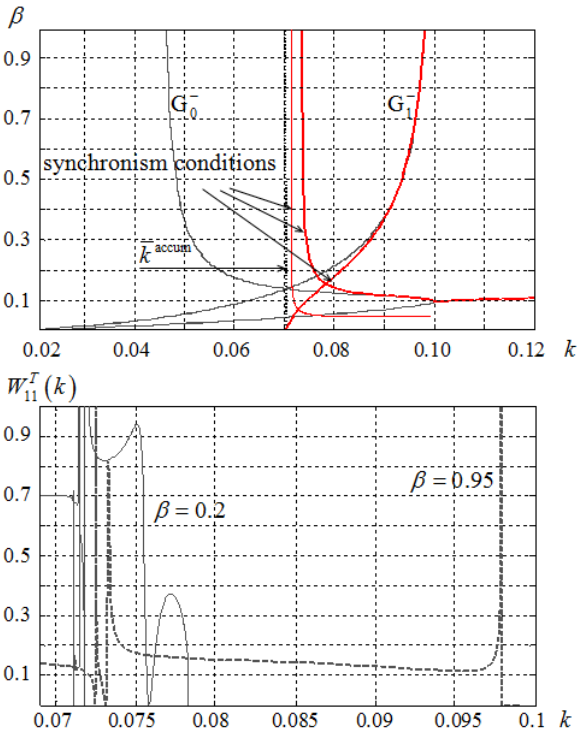

Figure 5. Same as in Figure 3, but for dispersive medium with parameters $k_{\varepsilon}=0.1,\ k_{\mu}=0.5$.

With the values $k_{\varepsilon}=0.1$ and $k_{\mu}=0.5$ comprising constitutive parameters of the dispersive medium, the range including the frequency intervals where Vavilov-

Cherenkov radiation can be observed for all $\beta \geq 0.14$ contains an accumulation point and from two to three points $\{k,\beta\}^{\text{synchr}}$ providing the fulfilment of one of the synchronism conditions (see Figure 5). In this parameter domain, the medium located below the periodic boundary is bi-negative. The values of the functions determining the radiation efficiency change especially sharply in the near vicinity of the point $k = \bar{k}^{\text{accum}}$ where for $\beta \geq 0.2$ two points $\{k,\beta\}^{\text{synchr}}$ fall into this vicinity. In the corresponding fragment of Figure 5, the functions $W_{11}^{T}(k)$ are truncated at the level $W_{11}^{T}(k) = 1$. Their maximum values, determined when observing the frequency range in increments of 0.00001, are 233.5004 for $\beta = 0.2$ and 6.426 for $\beta = 0.95$.

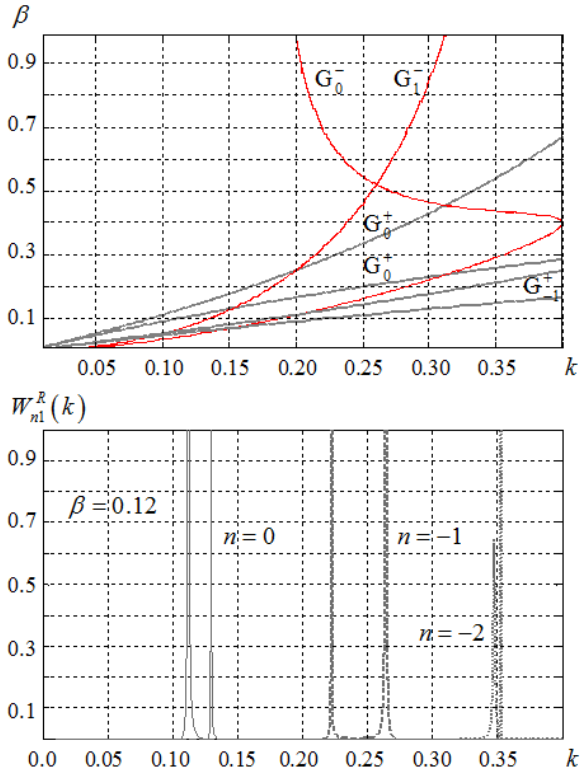

Figure 6. Smith-Purcell radiation into free space over dispersive medium with parameters $k_{\varepsilon} = 0.5$, $k_{\mu} = 0.4$ and sinusoidal boundary $z = f(y)$, $l = 2\pi$, $b = 0.4$.

The last of the results discussed in this section is related to the study of Smith-Purcell radiation on harmonics propagating in free space (in the zone $z > 0$). In Figure 6, the boundaries $G_n^{\pm}$ in coordinates k, β and functions $W_{n1}^R(k,\beta)$ (also truncated at $W_{n1}^R(k) = 1$) are presented for the case $k_\varepsilon = 0.5$, $k_\mu = 0.4$, $\beta = 0.12$, $n = 0, -1, -2$. Functions $W_{n1}^R(k,\beta)$ characterize the conversion efficiency of the electron flow field into the radiation field of the harmonic $\vec{U}_0^R(g,k)$ ($\max\limits_k W_{01}^R(k) \approx 1643$), and then, as k grows, into the field of the harmonic $\vec{U}_{-1}^R(g,k)$ ($\max\limits_k W_{-11}^R(k) \approx 50.5$), and further into the field of the harmonic $\vec{U}_{-2}^R(g,k)$ ($\max\limits_k W_{-21}^R(k) \approx 14353$). Such a sequence appears because the frequency intervals, where each of these harmonics propagates without attenuation, do not overlap each other when $\beta = 0.12$. The corresponding points of k, β plane do not fall into the Vavilov-Cherenkov radiation region. All the resonant bursts of functions $W_{n1}^R(k)$ occur in a small vicinity of points $\{k,\beta\}^{\text{synchr}}$ (in the viewed part of the plane of variables k and β they are located near the curves G_n^+), and the bursts are especially strong (in the case of $W_{-21}^R(k)$) in the area where one of the points $\{k,\beta\}^{\text{synchr}}$ is located near the accumulation frequency $k = \overline{k}^{\text{accum}} \approx 0.354$.

MODELS OF THE METHOD OF EXACT ABSORBING CONDITIONS

Consider a dielectric layer of finite thickness which is periodic along the y-axis and homogenous along the x-axis, Figure 7a. The field $\vec{U}^s(g,k) = \{\vec{E}^s(g,k), \vec{H}^s(g,k)\}$ is generated in the reflection ($z > 0$) and transition ($z < -h$) zones of this dielectric layer when excited by the homogenous ($\operatorname{Im}\Gamma_p = 0$) or inhomogeneous ($\operatorname{Im}\Gamma_p > 0$) plane wave $\vec{U}_p^i(g,k): H_x^i(g,k) = \exp(-i\Gamma_p z)\varphi_p(y)$. In particular, when $p = 1$ and $\Phi_1 = k/\beta$, it is excited by the field (1) of an electron beam with

$-2\pi\rho\beta\sqrt{l}\exp\left[-ka\sqrt{(1/\beta)^2-1}\right]=1$. According to the method of exact absorbing conditions, the amplitude coefficients $R_{np}(k)$ and $T_{np}(k)$ of the $\vec{U}^s(g,k)$ field's component

$$H_x^s(g,k)=\sum_{n=-\infty}^{\infty}\varphi_n(y)\begin{cases}R_{np}(k)\exp(i\Gamma_n z); & z\ge 0\\ T_{np}(k)\exp\left[-i\Gamma_n(z+h)\right]; & z\le -h\end{cases} \tag{15}$$

are determined from solution of the following correctly formulated [35,36] in the closure $\overline{\Omega}$ of the domain $\Omega=\{g=\{y,z\}:0<y<l,-h<z<0\}$ initial boundary value problem:

$$\begin{cases}\left[-\varepsilon(g)\partial_t^2-\sigma(g)\eta_0\partial_t+\partial_y^2+\partial_z^2\right]\mathrm{H}_x(g,t)=0; \quad g\in\Omega, \quad t>0\\ \mathrm{H}_x(g,0)=0, \quad \partial_t\mathrm{H}_x(g,t)\big|_{t=0}=0; \quad g=\{y,z\}\in\overline{\Omega}\\ \mathrm{H}_x(g,t) \text{ and } \vec{\mathrm{E}}_{tg}(q,t) \text{ are continuous when crossing } \Sigma^{\varepsilon,\sigma},\\ \quad \mathrm{H}_x\{\partial_y\mathrm{H}_x\}(l,z,t)=\exp(i2\pi\Phi)\mathrm{H}_x\{\partial_y\mathrm{H}_x\}(0,z,t) \quad \text{for} \quad -h<z<0,\\ \quad D^+\left[\mathrm{H}_x(g,t)-\mathrm{H}_x^i(g,t)\right]\big|_{g\in\mathrm{L}^+}=0 \quad \text{and} \quad D^-\left[\mathrm{H}_x(g,t)\right]\big|_{g\in\mathrm{L}^-}=0; \quad t\ge 0.\end{cases} \tag{16}$$

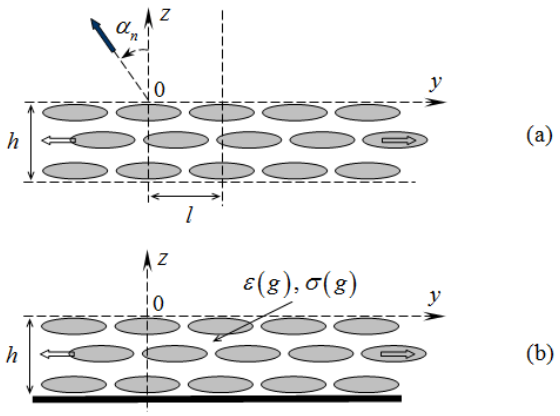

Figure 7. Structures with periodic interfaces: (a) dielectric layer of finite thickness, $\varepsilon(y,z)=\varepsilon(y+l,z)$ and $\sigma(y,z)=\sigma(y+l,z)$; (b) 2-D photonic crystal of limited thickness on metal substrate.

Here, $\mathrm{H}_x(g,t)$ is one of the three non-zero components of the total field

$$\vec{\mathrm{U}}(g,t)=\left\{\vec{\mathrm{E}}(g,t),\vec{\mathrm{H}}(g,t)\right\}=\begin{cases}\vec{\mathrm{U}}_p^i(g,t)+\vec{\mathrm{U}}^s(g,t); & z\geq 0\\ \vec{\mathrm{U}}^s(g,t); & z<0,\end{cases}$$

generated by the pulse wave $\vec{\mathrm{U}}_p^i(g,t)=\left\{\vec{\mathrm{E}}^i(g,t),\vec{\mathrm{H}}^i(g,t)\right\}$: $:\mathrm{H}_x^i(g,t)=v_p(z,t)\varphi_p(y)$, $z\geq 0$ (with its spectral components, we associate the fields of plane monochromatic waves $\vec{U}_p^i(g,k)$), and $\left[\varepsilon(g)\eta_0^{-1}\partial_t+\sigma(g)\right]\mathrm{E}_y(g,t)=\partial_z\mathrm{H}_x(g,t)$, $\left[\varepsilon(g)\eta_0^{-1}\partial_t+\sigma(g)\right]\mathrm{E}_z(g,t)=$ $=-\partial_y\mathrm{H}_x(g,t)$. Real-valued piecewise-constant functions $\varepsilon(g):\varepsilon(g)>0$, $\varepsilon(y,z)=\varepsilon(y+l,z)$ and $\sigma(g):\sigma(g)>0$, $\sigma(y,z)=\sigma(y+l,z)$ set the relative permittivity and conductivity of the layer $-h\leq z\leq 0$ of material; $\Sigma^{\varepsilon,\sigma}$ are the surfaces on which these functions have discontinuities. $D^+\left[\mathrm{H}_x(g,t)-\mathrm{H}_x^i(g,t)\right]\Big|_{g\in\mathrm{L}^+}=0$ and $D^-\left[\mathrm{H}_x(g,t)\right]\Big|_{g\in\mathrm{L}^-}=0$ are the exact absorbing conditions for pulse waves $\vec{\mathrm{U}}^s(g,t)$ generated by the wave $\vec{\mathrm{U}}_p^i(g,t)$ and propagating into the reflection and transition zones of periodic dielectric layer across the boundaries L^+ and L^- of the domain Ω in the planes $z=0$ and $z=-h$. The analytical form of these conditions used in this work is determined by the relations [29,31,33,35]

$$\begin{cases}\mathrm{H}_x(y,0,t)-\mathrm{H}_x^i(y,0,t)=-\sum\limits_{n=-\infty}^{\infty}\left\{\int\limits_0^t J_0\left[\Phi_0(t-\tau)\right]\times\right.\\ \quad\left.\times\left[\int\limits_0^l\partial_{\tilde{z}}\left[\mathrm{H}_x(\tilde{y},\tilde{z},\tau)-\mathrm{H}_x^i(\tilde{y},\tilde{z},\tau)\right]\Big|_{\tilde{z}=0}\varphi_n^*(\tilde{y})d\tilde{y}\right]d\tau\right\}\varphi_n(y),\\ \mathrm{H}_x(y,-h,t)=\sum\limits_{n=-\infty}^{\infty}\left\{\int\limits_0^t J_0\left[\Phi_0(t-\tau)\right]\left[\int\limits_0^l\partial_{\tilde{z}}\mathrm{H}_x(\tilde{y},\tilde{z},\tau)\Big|_{\tilde{z}=-h}\varphi_n^*(\tilde{y})d\tilde{y}\right]d\tau\right\}\varphi_n(y).\end{cases}$$

(17)

Here, $J_0(...)$ is the Bessel cylindrical function, $0 \le y \le l$, $t \ge 0$, and the asterisk $*$ stands for the complex conjugation.

Computational schemes for initial boundary value problems equipped with absorbing conditions of this type are stable. They quickly converge and lead to reliable and credible physical results in the numerical analysis of anomalous and resonant spatial-temporal and spatial-frequency transformations of electromagnetic waves [38,43]. The construction of exact absorbing conditions is the most difficult stage in the implementation of corresponding method for diverse and complex problems of computational electrodynamics. A brief history of this method and main analytical and physical results are presented in [12,23,29,31–38].

At the boundaries L^+ and L^- of the region Ω, the function $H_x^s(g,t)$ is represented by the following series of complete on the interval $0 \le y \le l$ orthonormal system of functions $\{\varphi_n(y)\}_{n=-\infty}^{\infty}$:

$$H_x^s(y,0,t) = \sum_{n=-\infty}^{\infty} u_{np}^+(t)\varphi_n(y), \quad H_x^s(y,-h,t) = \sum_{n=-\infty}^{\infty} u_{np}^-(t)\varphi_n(y).$$

The amplitude coefficients $R_{np}(k)$ and $T_{np}(k)$, which define all electrodynamic characteristics of the layer, are found from the relations [34,35]

$$R_{np}(k) = \tilde{u}_{np}^+(k)/\tilde{v}_1(0,k) \quad \text{and} \quad T_{np}(k) = \tilde{u}_{np}^-(k)/\tilde{v}_1(0,k). \tag{18}$$

Here, $\tilde{f}(k) = \int_0^T f(t)\exp(ikt)dt$, and T is the upper limit of the observation interval $0 \le t \le T$ in the numerical solution of the initial boundary value problem (16).

The elements $R_{np}(k)$ and $T_{np}(k)$ of the generalized scattering matrices $\{R_{np}(k)\}_{n,p=-\infty}^{\infty}$ and $\{T_{np}(k)\}_{n,p=-\infty}^{\infty}$ are related by the energy balance equations

$$\sum_{n=-\infty}^{\infty}\left[\left|R_{np}\right|^2 + \left|T_{np}\right|^2\right]\begin{Bmatrix}\operatorname{Re}\Gamma_n\\ \operatorname{Im}\Gamma_n\end{Bmatrix} = \begin{Bmatrix}\operatorname{Re}\Gamma_p + 2\operatorname{Im}R_{pp}\operatorname{Im}\Gamma_p\\ \operatorname{Im}\Gamma_p - 2\operatorname{Im}R_{pp}\operatorname{Re}\Gamma_p\end{Bmatrix} - \frac{k^2}{\mu_0}\begin{Bmatrix}W_1\\ W_2\end{Bmatrix} \tag{19}$$

and by the reciprocity relations

$$R_{np}(\Phi)/\Gamma_p(\Phi) = R_{-p,-n}(-\Phi)/\Gamma_{-n}(-\Phi), \tag{20}$$

which are the corollaries from the Pointing's complex power theorem and the Lorentz lemma [8,40]. In (19), we have used the following designations:

$$W_1 = \frac{\eta_0\varepsilon_0}{k}\int\limits_{\Omega}\sigma(g)\left|\vec{E}(g,k)\right|^2 dg \quad \text{and} \quad W_2 = \int\limits_{\Omega}\left[\varepsilon(g)\varepsilon_0\left|\vec{E}(g,k)\right|^2 - \mu_0\left|\vec{H}(g,k)\right|^2\right]dg.$$

Every harmonic $\vec{U}_n^R(g,k)$ or $\vec{U}_n^T(g,k)$ of the field $\vec{U}^s(g,k)$, for which $\operatorname{Im}\Gamma_n = 0$ and $\operatorname{Re}\Gamma_n > 0$, is a homogeneous plane wave propagating away from a grating at the angle $\alpha_n = -\arcsin(\Phi_n/k)$ into the reflection zone $z > 0$, and at the angle $\alpha_n = \pi + \arcsin(\Phi_n/k)$ into the transmission zone $z < -h$. All angles are measured anticlockwise from the z-axis in the $y0z$-plane, Figure 7a. For $\operatorname{Re}\Gamma_p > 0$, the angle $\alpha_p^i = \arcsin(\Phi_p/k)$ is the angle of incidence of the wave $\vec{U}_p^i(g,k)$ onto a grating. According to (19), the values

$$W_{\text{abs}}(k) = \frac{k^2}{\mu_0|\Gamma_p|}W_1, \quad W_{np}^R(k) = |R_{np}|^2\frac{\operatorname{Re}\Gamma_n}{|\Gamma_p|}, \quad W_{np}^T(k) = |T_{np}|^2\frac{\operatorname{Re}\Gamma_n}{|\Gamma_p|} \tag{21}$$

determine the relative part of energy lost to absorption and directed by a grating into the relevant spatial harmonic.

If a grating is excited by an inhomogeneous plane wave ($\operatorname{Im}\Gamma_p > 0$), the near-field to far-field conversion efficiency (diffraction radiation efficiency) is determined by the value of $\operatorname{Im}R_{pp}$ (see (19)), which in this case is non-negative and

$$2\operatorname{Im}R_{pp} = \sum_n\left(W_{np}^R + W_{np}^T\right) + W_{\text{abs}}. \tag{22}$$

As follows from (20) and the equalities $\Phi_n(\Phi) = -\Phi_{-n}(-\Phi)$ and $\Gamma_n(\Phi) = \Gamma_{-n}(-\Phi)$, one can study the excitation of a reflecting grating by an inhomogeneous plane wave in the context of conventional for the gratings theory diffraction problem: a structure is excited by a homogeneous plane wave

$\vec{U}^{i}_{-n}(g,k,-\Phi)$ and the coefficient $R_{-p,-n}(-\Phi)$ of conversion into damped spatial harmonic $\vec{U}^{R}_{-p}(g,k,-\Phi)$ is calculated.

We have described briefly the main points related to the application of the method of exact absorbing conditions for solving problems of diffraction of plane homogeneous and inhomogeneous waves $\vec{U}^{i}_{p}(g,k): H^{i}_{x}(g,k) = = \exp(-i\Gamma_{p} z)\varphi_{p}(y)$ by a periodic dielectric layer of finite thickness. The case of inhomogeneous waves ($\operatorname{Im}\Gamma_{p} > 0$) and, in particular, the case with $p = 1$, $\operatorname{Im}\Gamma_{1} > 0$, ($\Phi_{1} = k/\beta$) allows us to analyze the effects of diffraction radiation in a system 'density-modulated electron flow – periodic dielectric layer' using this method. Modifications that need to be made to allow the analysis of electrodynamic characteristics of the same layer on a perfect metal substrate (see Figure 7b) are obvious, and we will not dwell on them here.

INTERFACE 'VACUUM – 2-D PHOTONIC CRYSTAL'. NUMERICAL RESULTS

Consider a 2-D photonic crystal made of circular dielectric cylinders ($\varepsilon = 8.9$, $\sigma = 0$) with directrices parallel to the x-axis, Figure 8a. The axes of the cylinders at the intersection with the planes $x = const$ set the nodes of rectangular grid, which is infinite in the directions y and z, its cells' size is $l \times l$. The cylinder 's radius is $r = 0.38l$. The paper [37] is devoted to the determination of electrodynamic characteristics of such spatially bounded crystals when placed in a field of E-polarized waves. Below we discuss several issues related to the excitation of such structures (see Figure 7) by the field of a density-modulated electron flow (plane inhomogeneous H-polarized wave). First, we present some auxiliary results confirming that a layer cut from an ideal (infinite in all directions) photonic crystal retains basic properties of that crystal if layer's thickness is sufficient (but finite).

Let us cut out (by planes $z = const$) a grating from a photonic crystal. The grating's thickness h varies from $3l$ to $10l$ ($l = 2\pi$). The grating is excited with a normally incident ($\Phi = 0$) ultra-wideband H-polarized pulse

$$\vec{\mathrm{U}}_0^i(g,t):\mathrm{H}_x^i=v_0(z,t)\varphi_0(y);\quad v_0(0,t)=4\frac{\sin\left[\Delta k\left(t-\tilde{T}\right)\right]}{\left(t-\tilde{T}\right)}\cos\left[\tilde{k}\left(t-\tilde{T}\right)\right]\times \tag{23}$$

$$\times\chi\left(\overline{T}-t\right)=F_1(t),\quad \tilde{k}=0.5,\quad \Delta k=0.45,\quad \tilde{T}=150,\quad \overline{T}=300.$$

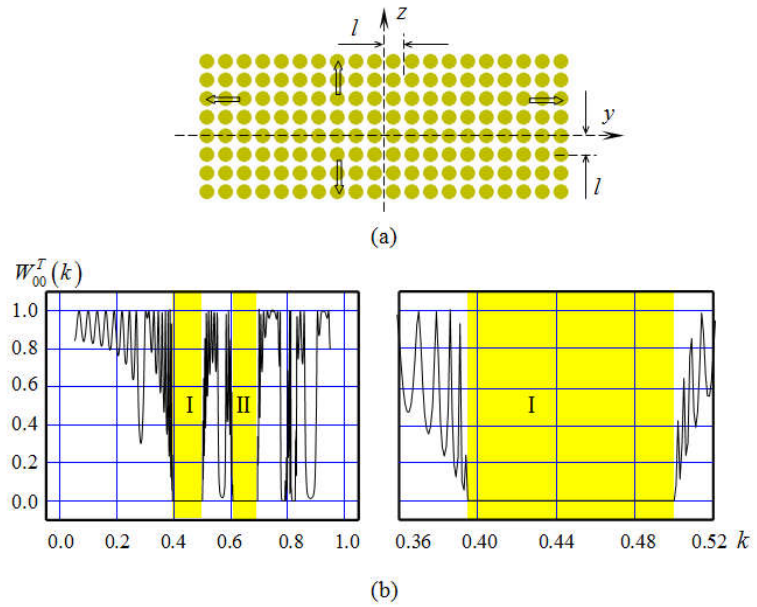

Figure 8. (a) 2-D photonic crystal. (b) Bandgaps (BGs) for the crystal of finite thickness: $h=10l$; $\Phi=0$.

Here, $\chi(...)$ is the Heaviside step function, the parameters $\tilde{k}$ and Δk set the central frequency of the pulse $F_1(t)$ and its band $\tilde{k}-\Delta k\le k\le\tilde{k}+\Delta k$ ($0.05\le k\le 0.95$), $\tilde{T}$ and $\overline{T}$ are delay and duration of the pulse $\vec{\mathrm{U}}_0^i(g,t)$ [32,34].

Within the frequency range $0.05\le k\le 0.95$, these gratings (we call them the gratings of finite thickness) operate in a single mode regime [8,17], namely there are only principal spatial harmonics propagating without decay (harmonics with $n=0$) in the reflection and transition zones. For the case $h=3l$, the band gaps' contours (BGs are frequency bands where $W_{00}^T(k)=0$) are only indicated (see, for example, Figure 3 in work [37]). But they are finally formed by structures containing 10 or more layers of thickness l each, Figure 8b. Before the left

boundary of the first such zone, up to the values of $k \approx 0.28$, a photonic crystal of thickness $h = 10l$ works as a homogenous dielectric plate, it is completely transparent for a normally incident plane wave at values k corresponding to half-wave resonances along its thickness.

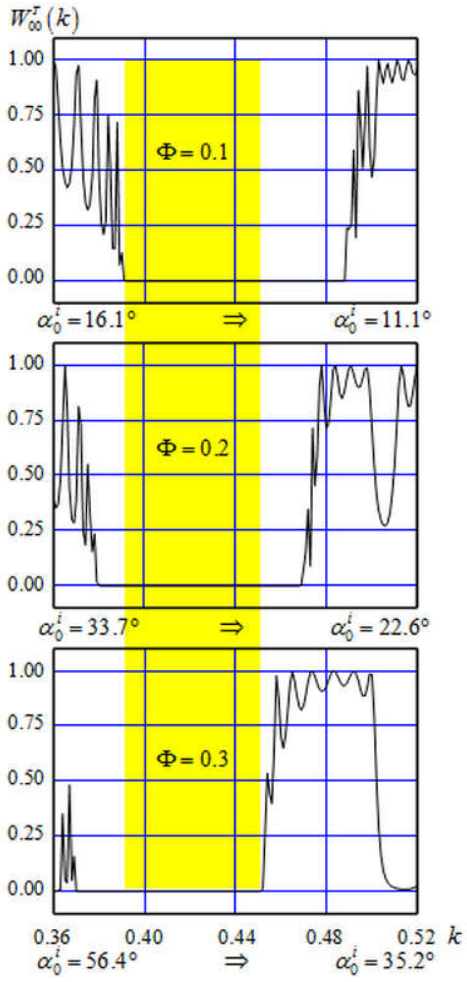

Figure 9. Drifting of the crystal's bandgap I with changing Φ (changing angle of incidence of the primary plane wave α_0^i).

Let's conduct a computational experiment same as described above, but for the pulse $\vec{U}_0^i(g,t)$ covering the frequency band $0.36 \le k \le 0.52$ and for $\Phi = 0.1$,

$\Phi = 0.2$, and $\Phi = 0.3$. It appears that with Φ increasing, the forbidden zone I is drifting towards smaller values of k with the width preserved, Figure 9. A larger value Φ corresponds to a larger value of the angle $\alpha_0^i = \arcsin\left(2\pi\Phi/lk\right)$ of the wave $\vec{U}_0^i\left(g,k\right)$ arrival onto the grating. Summarizing the information given in Figures 8a and 9, we can conclude that the crystal with thickness $10l$ does not transmit H-polarized waves, which arrive at the angles $0 \le \alpha_0^i \le 56.4°$ for all $0.395 \le k \le 0.455$ (the width $B_k = 2\left(k_{\text{upp}} - k_{\text{low}}\right)\Big/\left(k_{\text{upp}} + k_{\text{low}}\right) \times 100\%$ of this band is approximately equal to 14%).

Now excite the crystal with thickness $h = 10l$ with the pulse

$$\vec{\mathrm{U}}_1^i\left(g,t\right): \mathrm{H}_x^i = v_1\left(z,t\right)\varphi_1\left(y\right); \quad \Phi = 0, \quad v_1\left(0,t\right) = F_1\left(t\right), \\ \tilde{k} = 0.5, \quad \Delta k = 0.45, \quad \tilde{T} = 150, \quad \bar{T} = 300. \tag{24}$$

The pulse (24) covers the frequency band $0.05 \le k \le 0.95$, and in this case a homogenous plane wave $\vec{U}_1^i\left(g,k\right)$ corresponds to it: $\Phi_1 = k/\beta = 1.0$. The field of this wave is associated with the field of the electron flow. At that, the diffraction radiation is represented by harmonics $\vec{U}_0^R\left(g,k\right)$ and $\vec{U}_0^T\left(g,k\right)$, which go to infinity strictly normally to the periodic structure.

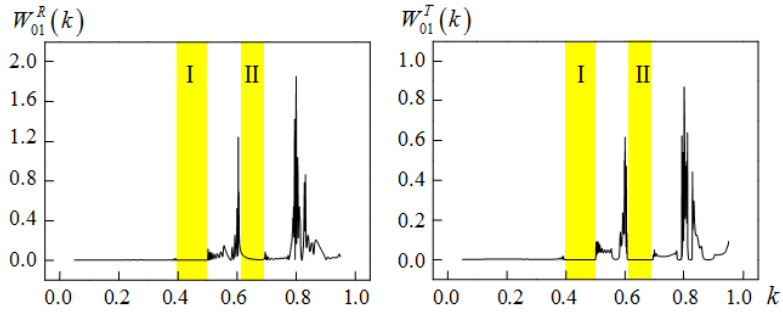

Figure 10. Efficiency of diffraction radiation into the reflection and transition zones of the crystal with finite thickness: $h = 10l$, $\Phi = 0$.

Up to the left boundary of the first forbidden band, the efficiency of wave $\vec{U}_1^i\left(g,k\right)$ transformation into propagating spatial harmonics of the crystal structure

(diffraction radiation efficiency) is practically zero (Figure 10). The diffraction radiation in the transmission zone is completely absent in the intervals of k variation corresponding to the bandgaps I and II. The value of $W_{01}^{R}(k)$ in these zones slightly differs from zero. We can confidently say that before the value $k \approx 0.5$ (and the value $\beta \approx 0.5$), the electron flow passing near the crystal limited in thickness generates in its reflection and transmission zones only inhomogeneous waves decaying exponentially with increase of the distance from the periodic boundaries 'vacuum – photon crystal'.

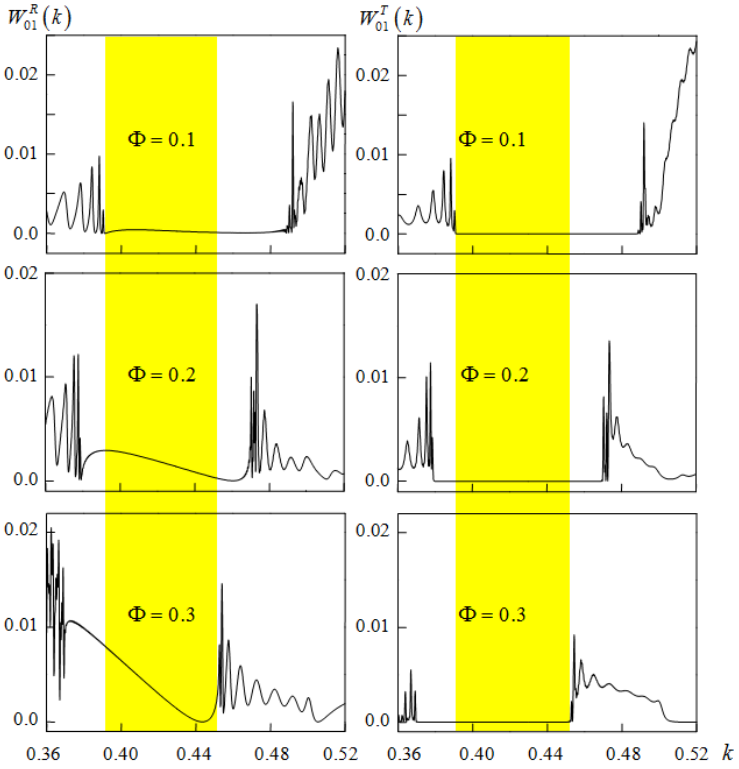

Figure 11. Efficiency of diffraction radiation into the reflection and transition zones of the crystal with thickness $h = 10l$ for $\Phi = 0.1$, $\Phi = 0.2$, and $\Phi = 0.3$.

The above-mentioned remains mostly valid and in cases when the parameter Φ is non-zero (Figure 11). The intervals of the frequency parameter k variation for which $W_{01}^{T}(k) = 0$ move with growth of Φ as well as the bandgaps of the

crystal; here the efficiency of diffraction radiation $W_{01}^{R}(k)$ slightly increases. The values $0.36 \le k \le 0.52$ correspond to the electron beam velocities $0.327 \le \beta \le 0.473$ for $\Phi = 0.1$, $0.3 \le \beta \le 0.433$ for $\Phi = 0.2$, and $0.277 \le k \le 0.4$ for $\Phi = 0.3$. The curves $W_{01}^{R}(k)$ and $W_{01}^{T}(k)$ presented in Figure 11 had been calculated for these parameters. For such values of k and β, the wave $\vec{U}_{0}^{R}(g,k)$ exit the crystal in its reflection zone at the angle $-16.13° \le \alpha_0 \le -11.09°$ for $\Phi = 0.1$, $-33.75° \le \alpha_0 \le -22.62°$ for $\Phi = 0.2$, and $-56.44° \le \alpha_0 \le -35.23°$ for $\Phi = 0.3$.

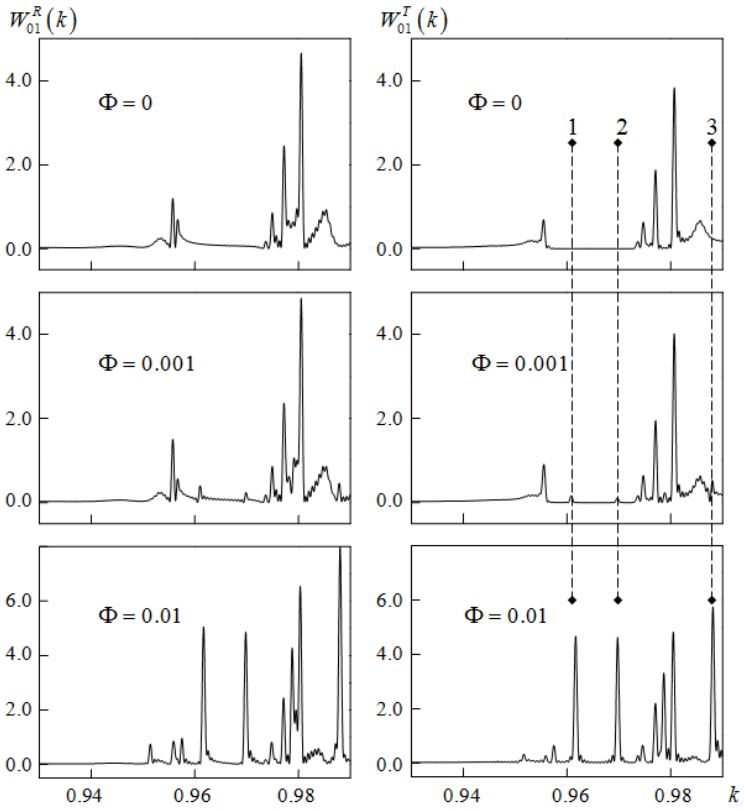

Figure 12. Relativistic electron flow. Efficiency of diffraction radiation near the normal to the flat interface ‘vacuum – crystal’: $h = 10l$.

The frequencies $0.93 \le k \le 0.99$ (see Figure 12) correspond to the relativistic velocities of electrons: $0.93 \le \beta \le 0.99$ for $\Phi = 0$, $0.929 \le k \le 0.989$ for $\Phi = 0.001$, and $0.921 \le \beta \le 0.98$ for $\Phi = 0.01$. With these values of k and β, $-0.62°$ is the maximum value of the angle α_0 between the normal to the periodic interface between the media and the direction of the wave $\vec{U}_0^R(g,k)$ when it exits the crystal into the reflection zone does. With k growth, the number M of waves propagating in the crystal and connecting its reflection and transmission zones also increases. It is known [8,17], that a pair of values $\{N,M\}$, where N is the number of spatial harmonics $\vec{U}_n^R(g,k)$ and $\vec{U}_n^T(g,k)$ propagating in the zones $z > 0$ and $z < -h$ without attenuation, is one of the most general characteristics of the processes of monochromatic waves scattering by periodic structures. The greater the difference $M - N$, the greater the number of resonances of various types involved in the formation of the grating response to any external excitation. As a rule, the energy characteristics $W_{01}^R(k)$ and $W_{01}^T(k)$ rush to their local or global extremes when one or another resonance occurs (this is due to the excitation of free oscillations of the field responsible for this resonance in the grating).

Free oscillations of the field $\vec{U}(g,\bar{k}_m) = \{\vec{E}(g,\bar{k}_m), \vec{H}(g,\bar{k}_m)\}$ (sometimes they are called eigen oscillations) in those periodic structures that are considered in this section, for any fixed real value Φ can exist for no more than a countable set of natural complex frequencies $\bar{k} \in \mathrm{K}$ without finite points of accumulation. Here, K is the Riemann surface, to which the solution of the stationary problem, corresponding to the initial boundary value problem (16), is analytically continued from real values of the frequency parameter k [8,40]. The Q-factor of the oscillation, corresponding to $\bar{k} = \mathrm{Re}\,\bar{k} + i\,\mathrm{Im}\,\bar{k}$, located in the first (physical) sheet of the surface K (here $\mathrm{Im}\,\bar{k} \le 0$ for all $\bar{k}$), is defined as $Q = \mathrm{Re}\,\bar{k} / 2\left|\mathrm{Im}\,\bar{k}\right|$.

The excitation of oscillations with sufficiently high Q (frequency of the exciting signal is $k \approx \mathrm{Re}\,\bar{k}$) leads to sharp (resonant) changes in the energy characteristics of the periodic structure. The result of these changes in the situation presented in Figure 12 are high enough values of $W_{01}^R(k)$ and $W_{01}^T(k)$ characterizing the efficiency of diffraction radiation.

Consider the occurrence and development of the resonances, indicated in Figure12 by the numbers 1, 2 and 3. The structure under consideration is symmetrical with respect to the planes $y = ml/2$, $m = 0, \pm 1, \pm 2, \ldots$ Therefore, when

it is excited by a wave $\vec{U}_1^i(g,k)$, in the case of $\Phi = 0$, in the corresponding part of space, the wave formations of two symmetry classes occur; but $\vec{U}_0^R(g,k)$ and $\vec{U}_0^T(g,k)$ belong only to one of them. In the wave formations belonging to this symmetry class, there are no free oscillations that could cause a resonance rise of the values $W_{01}^R(k)$ and $W_{01}^T(k)$ in the frequency interval $0.96 \le k \le 0.973$; here equality $W_{01}^T(k) \equiv 0$ holds. When passing to the values $\Phi \ne 0$, after corresponding changes in configuration of their field, the wave formations of two different classes of symmetry are combined into one general class of symmetry. In this class, there are already free oscillations, contributing to the resonant growth of $W_{01}^R(k)$ and $W_{01}^T(k)$ at the frequencies close to the real components $\mathrm{Re}\,\overline{k}$ of their eigen frequencies $\overline{k}$. In the case of resonance 1 (it occurs at the frequency $k = 0.96165$ for $\Phi = 0.01$), this is the oscillation under study, when the crystal is excited with the pulse

$$\vec{\mathrm{U}}_1^i(g,t):\mathrm{H}_x^i = v_1(z,t)\varphi_1(y);\quad \Phi = 0.01,\quad v_1(0,t) = \exp\left[-\left(t-\tilde{T}\right)^2 \Big/ 4\tilde{\alpha}^2\right]\times$$
$$\times\cos\left[\tilde{k}\left(t-\tilde{T}\right)\right]\chi\left(\overline{T}-t\right) = F_2(t), \tag{25}$$
$$\tilde{k} = 0.96165,\quad \tilde{\alpha} = 550,\quad \tilde{T} = 2500,\quad \overline{T} = 5000,\quad T = 15000.$$

This pulse covers a very narrow frequency band $0.95756 \le k \le 0.96574$ (the bandwidth is 0.85%), which does not include real values of eigen frequencies of other free field oscillations. Therefore, after turning off the source (25), the field of free oscillation dominates in the total field of the structure (Figure 13a), which causes the resonance under study. The behavior of the function $\mathrm{Re}\,u_{01}^+(t)\chi\left(t-\overline{T}\right)$, $t > \overline{T}$ (see Figure 13b) and the enveloping function $A\exp\left[\mathrm{Im}\,\overline{k}\left(t-\overline{T}\right)\right]$ define unambiguously the frequencies $\mathrm{Re}\,\overline{k} \approx 0.9617$, $\mathrm{Im}\,\overline{k} \approx -0.00105$ and $Q = \mathrm{Re}\,\overline{k}\big/2\left|\mathrm{Im}\,\overline{k}\right| \approx 460$ [34,44–46].

Now we shut the access to the crystal's transition zone with a metal substrate; the crystal thickness is $h = 10l$ (see Figure 2b), and it is excited by the pulse

$$\vec{\mathrm{U}}_1^i(g,t):\mathrm{H}_x^i=v_1(z,t)\varphi_1(y);\quad \Phi=0.1,\quad v_1(0,t)=F_1(t),\\ \tilde{k}=0.6,\quad \Delta k=0.5,\quad \tilde{T}=150,\quad \overline{T}=300, \tag{26}$$

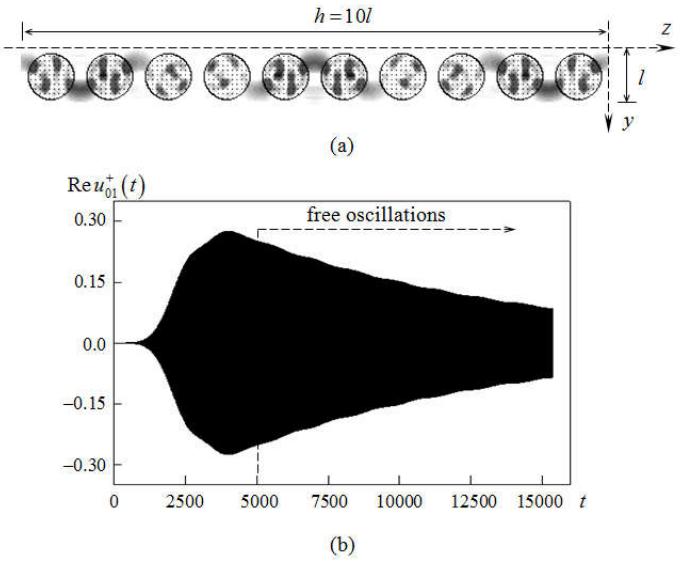

Figure 13. Excitation of the crystal structure by the pulse (25). (a) Pattern of $\mathrm{H}_x(g,t)$, $g\in\Omega$, $t=14000$ corresponding to eigen oscillation. (b) Behavior of $\mathrm{Re}\,u_{01}^{+}(t)$, $0\le t\le 15000$.

covering the band $0.1\le k\le 1.1$. In the interval $0.9\le k\le 1.1$ of this band, the wave $\vec{U}_1^i(g,k)$, whose field is identified with the field of electrons flying over a periodic structure with speed β, generates plane waves $\vec{U}_0^R(g,k)$ and $\vec{U}_{-1}^R(g,k)$, propagating in the direction of increasing z at the angles $\alpha_0(k)$ and $\alpha_{-1}(k)$. All principal characteristics of diffraction radiation, manifesting in this frequency range, are presented in Figure 14. On the frequency $k=0.9948$ (in Figure 14, the resonance 1 corresponds to this frequency), $W_{01}^R(k)\approx 0.07$ and $W_{-11}^R(k)\approx 5.0$, which means that almost all energy generated in the system 'crystal – electrons flow' is carried away into free space by the wave $\vec{U}_{-1}^R(g,k)$ ($\alpha_{-1}\approx 64.78°$ – reverse radiation). On the frequency $k=1.0668$ (in Figure 14, the resonance 2 corresponds

to it), $W_{01}^{R}(k) \approx 4.12$ and $W_{-11}^{R}(k) \approx 7.0$, which means that the generated energy is divided approximately in equal parts between the waves $\vec{U}_{0}^{R}(g,k)$ and $\vec{U}_{-1}^{R}(g,k)$, propagating from the periodic interface at the angles $\alpha_0 \approx -5.38°$ and $\alpha_{-1} \approx 57.53°$. On the frequency $k = 1.0728$ (in Figure 14, the resonance 3 corresponds to it), $W_{01}^{R}(k) \approx 11.6$ and $W_{-11}^{R}(k) \approx 2.1$, which means that the forward radiation $(\alpha_0 \approx -5.35°)$ is significantly more powerful than the reverse one $(\alpha_{-1} \approx 57.03°)$.

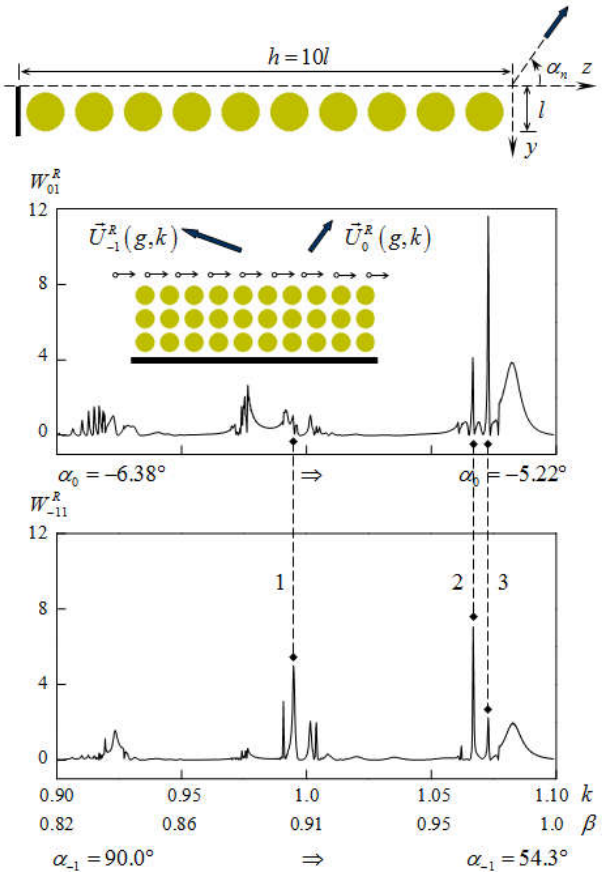

Figure 14. Characteristics of direct and reverse diffraction radiation in the system ‘electron flow – crystal on metal substrate’: $\Phi = 0.1$.

In the part of the frequency band $0.1 \le k \le 0.9$ covered by the pulse (26), the wave $\vec{U}_1^i(g,k)$ generates only one plane wave $\vec{U}_0^R(g,k)$, propagating at the angle $\alpha_0(k)$ in the direction of growing z. All principal characteristics of the effects of diffraction radiation are presented in Figure 15. Up to the first bandgap of the crystal, the magnitude $W_{01}^R(k)$ varies within the limits $0.0 \div 0.01$. For frequencies k from the first crystal's bandgap, the relation $W_{01}^R(k) \equiv 0$ holds. The frequencies of the second bandgap, in contrast, are characterized by sharp bursts of the $W_{01}^R(k)$ magnitude (up to $W_{01}^R(k) \approx 1.5$) at the left end of the band and at one of its inner sections, which are then replaced by intervals with a smooth change of $W_{01}^R(k)$ within $0.05 \div 0.15$ and within a section where $W_{01}^R(k) \equiv 0$. The highest value $W_{01}^R(k) = 6.21$ corresponds to the frequency $k = 0.8268$, the electron flow velocity $\beta \approx 0.752$, and the angle $\alpha_0 \approx -6.95^\circ$ of the $\vec{U}_0^R(g,k)$ wave's departure.

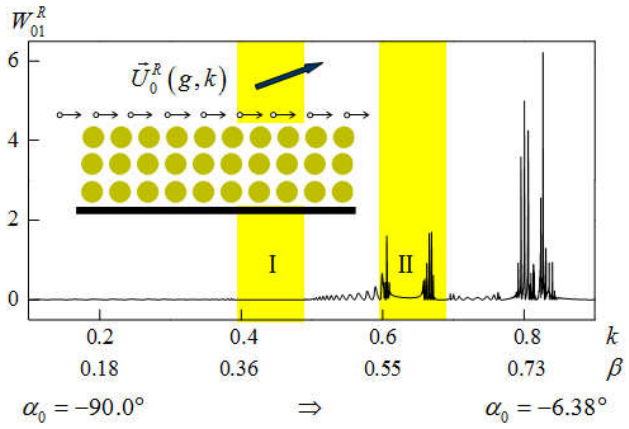

Figure 15. Regime of single-mode conversion of the inhomogeneous plane wave $\vec{U}_1^i(g,k)$ into the homogeneous wave $\vec{U}_0^R(g,k)$, propagating without attenuation in the reflection zone of the crystal on metal substrate: $\Phi = 0.1$.

PHOTONIC-CRYSTAL STRUCTURES FOR ELECTRON-WAVE SYSTEMS GENERATING THE SMITH-PURCELL RADIATION

One of the main technological problems arising in the creation of electronic devices for terahertz range is associated with the decrease in geometric dimensions of electrodynamic systems' elements and, in particular, with the decrease in periods of various retardation structures frequently used in such devices. New opportunities can be realized using the results of rapidly developing physics and technology of artificial media with unusual properties – photonic crystals. In such crystals, to allow interaction with an electron beam, the voids are arranged, and they have pronounced waveguide properties in bandgaps of an ideal periodic structure [37]. In addition, exploring such local crystals' defects, it is possible to create open resonant structures with rather high quality factors. Thus, a hollow channel in a photonic crystal (voids in crystal structure) can be used to transmit a linear electron flow. On frequencies outside of forbidden zones of a periodic structure, this flow will generate Smith-Purcell or Vavilov-Cherenkov radiation into space surrounding the channel. And on frequencies from forbidden zones, the electron flow will generate slow and fast waves running through the channel. Since at present there are sufficiently developed technologies for producing crystals with a characteristic cell size smaller than micron, it seems very promising to use these periodic structures in resonant and non-resonant terahertz devices. To do so, it is necessary to ensure that slow waves of a certain polarization exist in the waveguide channel of a crystal: if their phase velocity coincides with the electron flow speed (synchronism mode), the efficiency of diffraction radiation or the excitation efficiency of waves traveling along the channel increases manifold.

Calculations of dispersion diagrams for waves in regular and defected photonic crystals were made using the freely distributed MIT Photonic Bands software package, which is based on the plane wave method and is widely used for electrodynamic modeling of various photonic crystal. The simplest way to form a waveguide in an infinite photonic crystal is to create a linear defect, namely changes in physical properties of one or more elements in adjacent layers. Figures 16 and 17 show several versions of hollow waveguides suitable for the implementation of diffraction radiation generated by a flat density-modulated electron beam. Dispersion curves of guided waves in the forbidden zones (darkening and oblique shading) and transparency zones of corresponding regular photonic crystals are also presented in Figures 16 and 17. Here, Φ_y is the longitudinal propagation constants of H-polarized waves ($E_x = H_y = H_z = 0$) in a linear crystal with defects'

characteristic size a (a is distance between the axes of hollow circular cylinders of radius $r = 0.45a$ in a medium with permittivity $\varepsilon = 12.0$). Dashed tilted lines are the light lines, they separate domains that correspond to the bulk (fast) and surface (slow) wave regimes of photonic crystal waveguide. In the detailed images of the structures under consideration all the proportions are preserved.

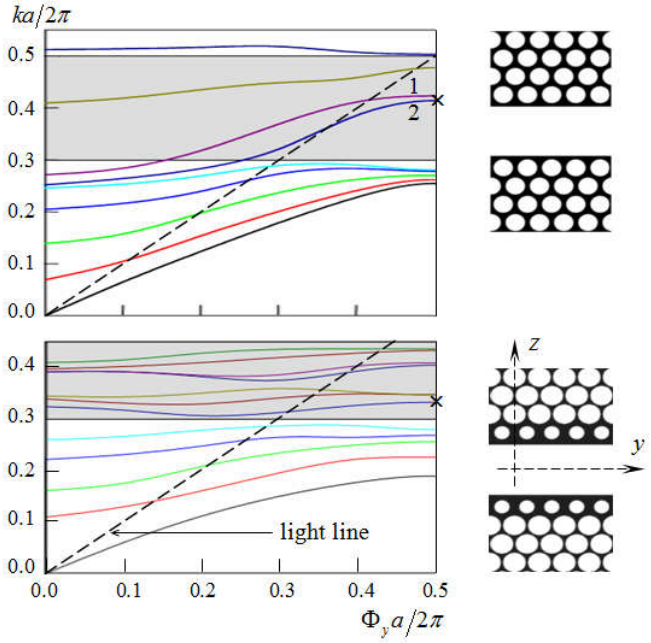

Figure 16. Dispersion characteristics of waveguiding channels in 2-D photonic crystal.

Calculations presented in [47–53] showed that the minimum phase velocity of slow eigen waves in channels with simple periodic boundaries, made by removing a plane-parallel layer of finite thickness from a crystal, is close to the velocity of light. To obtain a larger retardation rate for such waves, we changed configuration of periodic boundaries in several ways. Two of them are presented in Figures 16 and 17. In the lower fragment of Figure 16, hollow cylinders bordering the waveguide channel have smaller radius ($0.25a$) compared with elements of the regular part of the photonic crystal. As a result, it was possible to reduce the phase velocity $\beta = k/\Phi_y$ of the wave presented by the dispersion curve 1 from $\beta \approx 0.82$

(upper fragment) to $\beta \approx 0.64$ (lower fragment). The points on the plane of the variables k and Φ_y corresponding to this numerical experiment are marked with crosses in Figure 16.

The dispersion characteristics of the channel, which boundaries are lamellar gratings, are presented in Figure 17. For H -polarized waves, in the frequency range under consideration, the corresponding regular photonic crystal has two forbidden bands marked by oblique hatching. Dispersion curves crossing these zones correspond to the modes localized in the region of periodicity defect. Phase velocities of all slow waves are easily determined from the data given in Figure 17. Thus for the cross-marked point on the dispersion curve from the first bandgap of a regular crystal, the phase velocity of the corresponding surface wave is approximately equal to 0.68. Configuration of the wave field at this point ($E_y(y,z)$ pattern) is shown in the bottom of Figure 17 on the fragment 2. The fragment 1 shows configuration of the wave field from the second forbidden zone with propagation constant $\Phi_y a/2\pi = 0.44$. The corresponding dispersion curve is located closer to the low limit of forbidden zone.

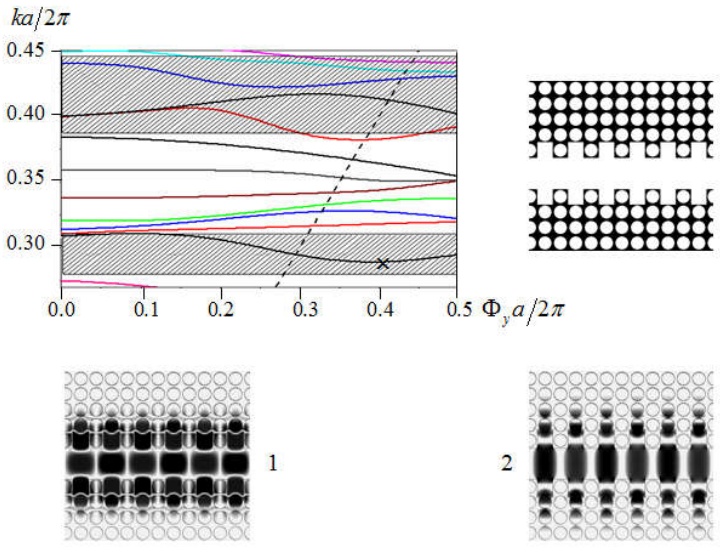

Figure 17. Same as in Figure 16, but for another geometry of waveguiding channel's periodic boundaries.

Symmetric (curve 1) and antisymmetric (curve 2) with respect to the plane $x0y$, bulk (fast) and surface (slow) modes are realized in the frequency region $3.0 < ka/2\pi < 4.5$ in the waveguide which dispersion characteristic are presented in the upper fragment of Figure 16. It should be noted that only symmetric modes can effectively interact with linear electron beams due to nonzero field intensity on the waveguide axis. Figure 18 shows spatial transverse distributions of the electric field longitudinal component E_y corresponding to this modes in the points where $\Phi_y a/2\pi = 0.45$. Vertical dashed lines indicate the boundaries of waveguide hollow channel. Field intensity drastically decreases within two periods of the photonic crystal waveguide boundary. Maximum intensity of electric field occurs on the boundaries of waveguide channel. Electric field value for the symmetric mode on the waveguide channel axis is about two times less than maximum value on the boundaries of hollow channel. Therefore, an electron beam occupying one half of the channel width can provide sufficient interaction impedance.

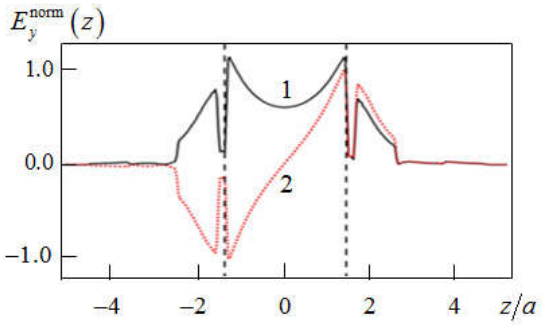

Figure 18. Longitudinal components of the slow waves' electric field represented by the dispersion curves 1 and 2 on the upper fragment of Figure 16 in the cross section of corresponding waveguide channel.

So, 2-D photonic crystals waveguides with different configurations of hollow channel periodic boundaries are investigated. Dispersion characteristics of these waveguides are calculated. The focus was set on slow wave modes in bandgaps of photonic crystals. Beams of charged particles interact with those modes only in devices implementing the excitation of slow and fast electromagnetic waves traveling through channels.

THE FINE STRUCTURE OF SMITH-PURCELL RADIATION

In the final section of this chapter, we present experimental results that reveal several not yet mentioned details important for the design of real-world systems with Smith-Purcell radiation. That is the question of so-called 'fine structure of diffraction radiation', which is usually out of consideration when solving many applied problems, and this may lead to results that are very far from expected ones. This phenomenon appears because an electron flow moving with speed β, which is modulated by a high-frequency field and focused by a magnetic field, generates not only the wave exciting a periodic structure, but a combination of waves which includes space-charge waves (SCWs) and cyclotron waves (CWs). The SCWs and CWs phase velocities, $\beta_{\pm m}^{\text{scw}}$ and $\beta_{\pm m}^{\text{cw}}$, are determined by the relations

$$\beta_{\pm m}^{\text{scw}} = \beta \Big/ \left(1 \pm \omega^{\text{plasma}} \omega^{-1}\right) < 1 \quad \text{and} \quad \beta_{\pm m}^{\text{cw}} = \beta \Big/ \left(1 \pm m\omega^{\text{cyclotr}} \omega^{-1}\right) < 1 . \tag{27}$$

Here, m is the number of a cyclotron wave (with $m = 0$ that is so-called synchronic electron wave, SEW), ω^{plasma} and ω^{cyclotr} are the plasma and cyclotron frequencies, ω is a frequency corresponding to the wavenumber k. ω^{plasma} is proportional to the square root of the current density divided by β, and ω^{cyclotr} is proportional to the external magnetic field induction. It is clear that each of these waves generate its own radiation field consisting of propagating harmonics $\vec{U}_n^R\left(g, k, \tilde{\beta}\right)$ (n is such that $\operatorname{Re}\Gamma_n\left(k, \tilde{\beta}\right) > 0$) when moving with different phase velocities $\tilde{\beta}$ over a reflective, for example, periodic (with period l) structure. Supposing, same as before, $\Phi_1 = 2\pi/l\left(1 + \Phi\right) = k/\tilde{\beta}$, we derive $\Phi_n = 2\pi/l\left(n + \Phi\right) = \Phi_1 + 2\pi\left(n-1\right)/l$ and formulate the condition guaranteeing that a harmonic with the number n will be propagating: $k > \left|k/\tilde{\beta} + 2\pi\left(n-1\right)/l\right|$. It is obvious that this can only be a harmonic with a non-positive number. The angle $\alpha_n\left(k, \tilde{\beta}\right)$, at which this harmonic exits the grating, is determined by the relation (see previous sections) $\alpha_n\left(k, \tilde{\beta}\right) = -\arcsin\left(\Phi_n/k\right) = \ = -\arcsin\left(1/\tilde{\beta} + 2\pi\left(n-1\right)/kl\right)$.

Differences in the spatial orientation of harmonics corresponding to different waves associated with a density-modulated and focused electron beam allow experimental studies of the fine structure of generated field. For millimeter waves, it was first recorded and studied in details in 1982–1987 [54–58]. The obtained

results significantly changed the concept of both the spatial-angular distribution and the polarization characteristics of radiation field. For the first time peculiarities in radiation processes associated with the magnitude and direction of magnetic field focusing an electron beam have been also investigated. We note that the question of the influence of space charge waves on characteristics of Smith-Purcell radiation have been raised earlier in [20], but the authors concluded that due to low density of electron current in the optical range, the corresponding effects may be neglected.

Electrons generating cyclotron waves are twisted into a spiral, which moves forward with the speed β and rotates in a fixed cross-section with the frequency ω^{cyclotr} [59]. This affects polarization characteristics of the radiation field corresponding to such waves.

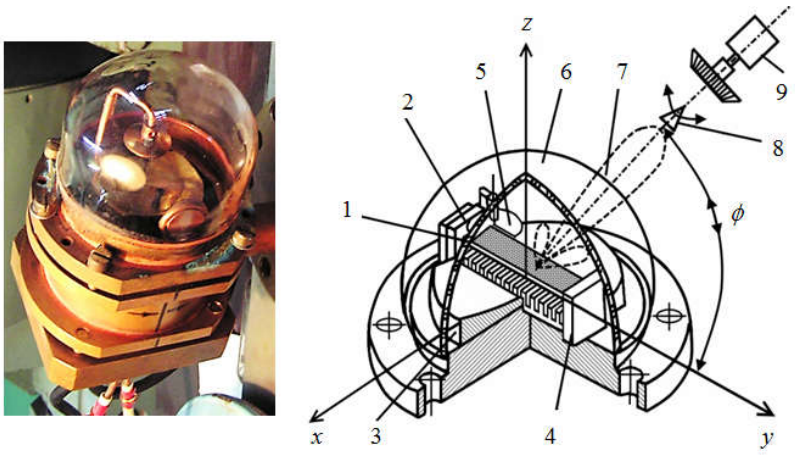

Figure 19. Electron-vacuum unit of the experimental setup and its schematic representation.

An experimental study of an electron beam radiation in the millimeter wavelength range have been carried out on a quasi-optical complex described in [56] (see also Figure 19). The complex was placed in the gap of a focusing electromagnet $70mm$ in length. The measurements have been carried out according to the following scheme. The tape-shaped electron beam 1 with the cross section $3.8\times 0.1mm^2$ and the current density less than $50\,A/cm^2$ was formed by the electron gun 2 with the accelerating voltage $1.0\div 4.0kV$, and after passing near the reflective grating 3 (lamellar grating with period $l=0.4mm$ and length $40mm$) was deposited on the collector 4. The beam was focused by magnetic field, which

induction could be changed within the interval $0.08 \div 0.5T$ in the central part of the gap. There was also the possibility of reversing the direction of the magnetic induction vector. The electron flow was modulated by the short-focus, compact diffraction radiation generator with a spherical mirror 5 (radius of the mirror is $15mm$) and a segment of the diffraction grating $18mm$ in length. The modulator was tuned by changing the distance between the grating and the spherical mirror.

The radiation investigated in the experiment was generated by the diffraction of the density-modulated electron beam field by a part of the reflective grating $22mm$ in length, not related to the modulator. Structurally, the modulator, the grating, the electron gun and the collector are in vacuum inside the thin-walled hemisphere glass cylinder 6, which center is aligned with the grating's center. The measuring unit of the complex enabled the determination of the following principal characteristics of the diffraction radiation 7: the angle ϕ between the direction of the electron beam velocity vector and the direction of the radiation wave propagation in the plane $y0z$, the orientation and width of corresponding lobe of radiation pattern, the polarization state of the radiated field, and the radiation power. The interval of measured values ϕ was limited by the electromagnet coils and was $50 \div 130°$. The error of angular measurements did not exceed $0.5°$. The angle of rotation of the polarization plane of the radiated field was set with $\pm 5'$ accuracy. The velocity β of the electron flow was regulated by the anode voltage of the gun and the frequency of modulation k ($f = 48 \div 80GHz$), via mechanical adjustment of the mirror 5 position. The polarization analyzer consisted of the conical horn 8, a waveguide junction connected to it with the rotating section 9 loaded onto a semiconductor amplitude modulator, and a crystal detector with an indicator. The measurement error of the orientation angle of the polarization ellipse was about 1°. The maximum intensity in certain lobes of the diagram peaked $1.0 \div 3.0 mW/cm^2$. To eliminate the reflections of the wave emitted from the device, metal surfaces of the installation have been shielded with an absorbing material.

In the general case, a multilobe structure was observed, due to the excitation of electron waves in the electron beam in the measured patterns of diffraction radiation. At currents of the order $30 A/cm^2$ and the focusing magnetic fields of $0.25 \div 0.5T$, the difference between the angles of radiation excited by fast (minus sign) and slow (plus sign) spatial charge waves propagating in the stream was equal to $15 \div 25°$, and for SCWs and synchronic electron waves was equal to $8 \div 12°$. Mechanical adjustments of the modulator provided the excitation of radiation by one or several electron waves at fixed electron beam velocity β.

In one of the experiments with the accelerating voltage $1100V$ and the frequency $f = 52.6GHz$ in the working range of angles ϕ, the radiation was excited by two electron waves, namely fast SCW and SEW. For the voltage $2255V$ and $f = 67.5GHz$, the radiation was excited only by slow SCW. For the voltage $2545V$ and $f = 75.0GHz$, there were three lobes corresponding to the excitation of radiation of slow SCW ($\phi \approx 71°$), fast SCW ($\phi \approx 94°$), and SEW ($\phi \approx 83°$) in the radiation pattern. The measured radiation angles were somewhat different from the theoretical ones, which is obviously caused by the reduction of plasma frequency due to finite dimensions of the electron beam, and the measurement error.

We have studied experimentally the change in intensity of slow SCW radiation and the magnitude of the angle γ between the major axis of polarization ellipse of the radiated field and the electron velocity vector when the accelerating voltage changes within the modulator generation zone $2180 \div 2350V$. In this experiment, the ellipticity coefficient varied within the interval $0.0 \div 0.15$ for the entire range the accelerating voltage, i.e. the polarization remained almost linear. Significant changes of γ occurred in the regime of soft generation. The range of γ variation decreased when the amplitude of the field in the modulator increased. The increasing accelerating voltage sets the value of γ at its minimum $\gamma = 12 \div 15°$. With the decrease in the electron current density, the range of γ over the generation zone of the modulator decreased while maintaining the general form of the corresponding dependence. The small deviation in the radiation field polarization from H-polarization is apparently due to the contribution of cyclotron (transverse) electron waves to this radiation. This assumption is confirmed by experimental studies of the influence of focusing magnetic field on the polarization state of diffraction radiation. It has been established that with increasing magnetic field $\vec{H}$, the angle γ for radiation generated by fast and slow SCWs increases and depends on the direction of $\vec{H}$. A characteristic feature of the results obtained is the presence of a jump in the orientation of the polarization plane of radiation when the direction of the focusing magnetic field is reversed.

A distinctive feature of synchronic electron waves is the fact that they propagate with the phase velocity β, and it is difficult to detect or identify them using diffraction radiation patterns. However, a theoretical analysis showed [55] that under the influence of a space charge, SEWs can be split into left- and right-polarized waves with separated values of phase velocities (fast and slow SEWs). The implementation of this possibility has been confirmed experimentally. It is shown that with well-defined relations between the current density and the

magnitude of the focusing magnetic field in the electron stream, one can detect the presence of two SEWs differing in the amplitude and polarization structure. The orientation γ of the polarization ellipses for these signals was almost the same in magnitude and opposite in sign. When studying the behavior of γ and the ellipticity coefficient in parameters region corresponding to the splitting, it was found that the high sensitivity of ellipticity coefficient to changes in the beam parameters is a feature distinguishing the radiation field generated by SEWs from the field generated by spatial charge waves.

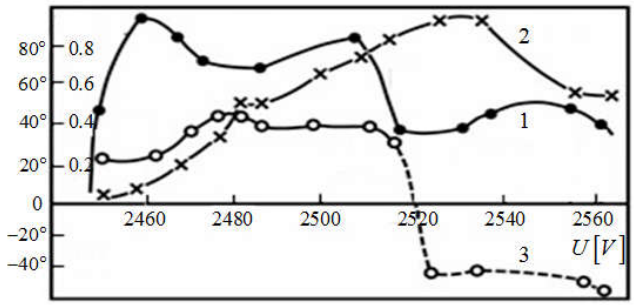

Figure 20. Normalized power (curve 1), the ellipticity coefficient (curve 2), and the rotation angle γ of polarization ellipse (curve 3) of the SWEs' radiation field when the accelerating voltage U is changing.

The statement is confirmed by the results presented in Figure 20. The ellipticity coefficient varied from 0.01 to 1.0, and the radiation field polarization changed from linear to circular. As the accelerating voltage rises, slow SEW ($\gamma = 20 \div 40°$) was excited first, and then, when going through the dip ($U \approx 2520V$) associated with the splitting, fast SEW ($\gamma = -20 \div -40°$) is excited too. The arrangement of polarization planes in main lobes of the diffraction radiation pattern, which is symmetric with respect to the motion path of unperturbed electrons, suggests that in this experiment we observed the fine structure of diffraction radiation caused by the excitation of synchronous electron waves, SEWs. The orientation angle γ of the polarization ellipse of their radiation field depends on magnitude and direction of the focusing magnetic field.

CONCLUSION

An electron flow moving near any periodic structure is a common thing in many instruments and devices of vacuum electronics and, in general, is already rather well-studied [2,20,21,47]. Here, in this chapter, we study peculiar features of this problem, which are specified by properties of materials used to construct periodic structures interacting with the flow. These are artificial materials that exhibit electromagnetic properties which are not observed in natural, traditional materials. And the main point of this work is to demonstrate the possibility to simulate accurately the interaction of moving charged particle beams with structures made of such materials, and the possibility to obtain reliable information about features of spatial-temporal and spatial-frequency transformations of electromagnetic waves associated with this interaction. A density-modulated electron beam moving near a periodic boundary dividing natural and artificial media generates Smith-Purcell or Vavilov-Cherenkov radiation. A number of physical system where such radiation occurs are detailed in the chapter, including plasma-like medium and photonic crystals bordered with vacuum. A significant part of the chapter is devoted to the fine structure of Smith-Purcell radiation, it is an important, but often overlooked topic. Problems of numerical modeling and analysis of Smith-Purcell and Vavilov-Cherenkov radiation are considered in this chapter within the framework of the given current approximation. To avoid disadvantages of this approximation, the authors have already developed and tested methods of frequency and time domains, which are based on the same principles as the methods that have been briefly described above.

REFERENCES

1. Smith, Steve, and Edward Purcell. 1953. “Visible Light from Localized Surface Charges Moving Across a Grating.” *Physical Review* 92(4):1069–73.
2. Shestopalov, Viktor. 1998. *The Smith-Purcell Effect*. New York: Nova Science Publishes Inc.
3. Cherenkov, Pavel. 1937. “Visible Radiation Produced by Electrons Moving in a Medium with Velocities Exceeding that of Light.” *Physical Review* 52:378–79.
4. Jelley, John. 1958. *Cherenkov Radiation and its Applications*. London: Pergamon Press.
5. Frank, Il’ya. 1988. *Vavilov-Cherenkov Radiation*. Moscow: Nauka.

6. Budanov, Valentin, *et al*. 1977. *Characteristics of Diffraction Radiation of Different Reflecting Gratings*. Kharkiv: IRE, Academy of Sciences of Ukraine, Preprint no.83.
7. Masalov, Sergey. 1980. "On a Possibility of Using an Echelette in the Diffraction Radiation Generators." *Ukrainskiy Fizicheskiy Zhurnal* 25(4):570–74 (in Russian).
8. Shestopalov, Viktor, and Yuriy Sirenko. 1989. *Dynamic Theory of Gratings*. Kyiv: Naukova Dumka.
9. Sirenko, Yuriy, and Lyudmyla Velychko. 2001. "The Features of Resonant Scattering of Plane Inhomogeneous Waves by Gratings: Model Problem for Relativistic Diffraction Electronics." *Telecommunications and Radio Engineering* 55(3):33–39.
10. Granet, Gerard, *et al*. 2015. "Resonances in Reverse Vavilov-Cherenkov Radiation Produced by Electron Beam Passage over Periodic Interface." *International Journal of Antennas and Propagation* 2015:ID 784204.
11. Sautbekov, Seil, *et al*. 2015. "Diffraction Radiation Effects: A Theoretical and Experimental Study." *Antennas and Propagation Magazine, IEEE* 57(5):73–93.
12. Sautbekov, Seil, *et al*. 2016. "Diffraction Radiation Phenomena: Physical Analysis and Application," In *Electromagnetic waves in Complex Systems. Selected Theoretical and Applied Problems*, edited by Yuriy Sirenko, and Lyudmyla Velychko, 387–442. New York: Springer.
13. Agranovich, Zalman, Marchenko, Volodymyr, and Viktor Shestopalov. 1962. "Diffraction of Electromagnetic Waves on Plane Metal Gratings." *Zhurnal Tekhnicheskoi Fiziki* 32:381–94.
14. Shestopalov, Viktor. 1971. *The Method of the Riemann-Hilbert Problem in the Theory of Electromagnetic Wave Diffraction and Propagation*. Kharkiv: Kharkiv State University Press.
15. Shestopalov, Viktor, et al. 1973. *Wave Diffraction by Gratings*. Kharkiv: Kharkiv State University Press.
16. Shestopalov, Viktor, Kirilenko, Anatoliy, and Sergey Masalov. 1984. *Matrix Convolution-Type Equations in the Diffraction Theory*. Kyiv: Naukova Dumka.
17. Shestopalov, Viktor, *et al*. 1986. *Resonance Wave Scattering. Diffraction Gratings*. Kyiv: Naukova Dumka.
18. Shestopalov, Viktor, *et al*. 1997. *New Solution Methods for Direct and Inverse Problems of the Diffraction Theory. Analytical Regularization of the Boundary Value Problems in Electromagnetic Theory*. Kharkiv: Osnova.

19. Melezhik, Petro, *et al*. 2010. “Analytic Regularization Method.” In *Modern Theory of Gratings. Resonant Scattering: Analysis Techniques and Phenomena*, edited by Yuriy Sirenko and Staffan Strom, 43–172. New York: Springer.
20. Shestopalov, Viktor. 1976. *Diffraction Electronics*. Kharkiv: Vyscha Shkola.
21. Shestopalov, Viktor, *et al*. 1991. *Diffraction Radiation Generators*. Kyiv: Naukova Dumka.
22. Yevdokymov, Anatoliy. 2013. “Diffraction Radiation Antennas.” *Fizicheskie Osnovy Priborostroenija* 2(1):108–25.
23. Melezhik, Petro, *et al*. 2018. “Cherenkov Radiation Based Antenna with the Funnel-Shaped Directional Pattern.” *Electromagnetics* 38(1):34–44.
24. Yevdokymov, Anatoliy, *et al*. 2018. . “Antennas of Diffraction Radiation on the Basis of a Groove Transmission Line.” *Fizicheskie Osnovy Priborostroenija* 7(1):24–36.
25. Sirenko, Kostyantyn, Sirenko, Yuriy, and Anatoliy Yevdokymov. 2018. “Diffraction Antennas. A Ridged Dielectric Waveguide.” *Telecommunications and Radio Engineering* 77(10):839–52.
26. Sautbekov, Seil, *et al*. 2018. “Diffraction Antennas. Synthesis of Radiating Elements.” *Telecommunications and Radio Engineering* 77(11):925–43.
27. Sirenko, Yuriy, and Anatoliy Yevdokymov. 2018. “Diffraction Antennas. Linear Structures on the Basis of a Ridged Waveguide.” *Telecommunications and Radio Engineering* 77(14):1203–29.
28. Mazur, Volodymyr, *et al*. 2018. “Diffraction Antennas. Linear Structures on the Basis of a Modified Goubau Line.” *Telecommunications and Radio Engineering* 77(16):1397–408.
29. Perov, Andrey, Sirenko, Yuriy, and Nataliya Yashina. 1999. “Explicit Conditions for Virtual Boundaries in Initial Boundary Value Problems in the Theory of Wave Scattering.” *Journal of Electromagnetic Waves and Applications* 13(10):1343–71.
30. Sirenko, Yuriy, and Nayaliya Yashina. 2003. “Time Domain Theory of Open Waveguide Resonators: Canonical Problems and a Generalized Matrix Technique.” *Radio Science* 38:VIC 26-1–VIC 26-12.
31. Sirenko, Konstyantyn, and Yuriy Sirenko. 2005. “Exact ‘Absorbing’ Conditions in the Initial Boundary Value Problems of the Theory of Open Waveguide Resonators.” *Computational Mathematics and Mathematical Physics* 45:490–506.
32. Sirenko, Yuriy, Strom, Staffan, and Nataliya Yashina. 2007. *Modeling and Analysis of Transient Processes in Open Resonant Structures. New Methods and Techniques*. New York: Springer.

33. Sirenko, Kostyantyn, Sirenko, Yuriy, and Nataliya Yashina. 2010. "Modeling and Analysis of Transients in Periodic Gratings. I. Fully Absorbing Boundaries for 2-D Open Problems." *Journal of the Optical Society of America A* 27:532–43.
34. Kravchenko, Viktor, Sirenko, Kostyantyn, and Yuriy Sirenko. 2011. *Electromagnetic Wave Transformation and Radiation by the Open Resonant Structures. Modeling and Analysis of Transient and Steady-State Processes*. Moscow: Fizmathlit.
35. Sirenko, Yuriy, Strom, Staffan, and Nataliya Yashina. 2010. "Modeling and Analysis of Transients in Periodic Structures: Fully Absorbing Boundaries for 2-D Open Problems." In *Modern Theory of Gratings. Resonant Scattering: Analysis Techniques and Phenomena*, edited by Yuriy Sirenko and Staffan Strom, 211–334. New York: Springer.
36. Sirenko, Kostyantyn, and Yuriy Sirenko. 2016. "The Exact Absorbing Conditions Method in the Analysis of Open Electrodynamic Structures." In *Electromagnetic waves in Complex Systems. Selected Theoretical and Applied Problems*, edited by Yuriy Sirenko, and Lyudmyla Velychko, 225–326. New York: Springer.
37. Ney, Michel, *et al*. 2017. "2-D Photonic Crystals: Electromagnetic Models of the Method of Exact Absorbing Conditions." *Telecommunications and Radio Engineering* 76(3):185–207.
38. Pazynin, Vadim, *et al*. 2017. "The Exact Absorbing Conditions in Initial Boundary Value Problems of Computational Electrodynamics. Survey." *Fizicheskie Osnovy Priborostroenija* 6(4):4–35.
39. Tretyakov, Oleg, Tretyakova, Svitlana, and Viktor Shestopalov. 1965. "Electromagnetic Wave Radiation by Electron beam Mowing over Diffraction Grating." *Radiotehnika I Elektronika* 10(7):1233–43.
40. Sirenko, Yuriy. 2010. "Basic Statements." In *Modern Theory of Gratings. Resonant Scattering: Analysis Techniques and Phenomena*, edited by Yuriy Sirenko and Staffan Strom, 1–42. New York: Springer.
41. Melezhik, Petro, *et al*. 2006. "Radiation from Surface with Periodic Boundary of Metamaterials Excited by a Current." *Progress In Electromagnetics Research* 65:1–14.
42. Melezhik, Petro, *et al*. 2007. "Periodic Boundary of Metamaterial: Eigen Regimes and Resonant Radiation." *Journal of Optics A*: *Pure and Applied Optics* 9:403–09.
43. Sirenko, Kostyantyn, *et al*. 2018. "Comparison of Exact and Approximate Absorbing Conditions for Initial Boundary Value Problems of the

Electromagnetic Theory of Gratings." *Telecommunications and Radio Engineering* 77(18):1581–95.

44. Sirenko, Yuriy, Velychko, Lyudmyla, and Fatih Erden. 2004. "Time-Domain and Frequency-Domain Methods Combined in the Study of Open Resonance Structures of Complex Geometry." *Progress In Electromagnetics Research* 44:57–79.
45. Velychko, Lyudmyla, Sirenko, Yuriy, and Olena Velychko. 2006. "Time-Domain Analysis of Open Resonators. Analytical Grounds." *Progress In Electromagnetics Research* 61:1–26.
46. Velychko, Lyudmyla, and Yuriy Sirenko. 2009. "Controlled Changes in Spectra of Open Quasi-Optical Resonators." *Progress In Electromagnetics Research B* 16:85–105.
47. Shmat'ko, Alexandr. 2008. *Electron-Wave Systems of the Millimeter Range. Vol.1*. Kharkiv: Kharkiv National University Press.
48. Odarenko, Evgeniy, and Alexandr Shmat'ko. 2016. "Photonic Crystal and Bragg Waveguides for THz Electron Devices." Paper presented at the IEEE International Conference on Laser and Fiber-Optical Networks Modeling, Odessa, Ukraine, September 12–15.
49. Odarenko, Evgeniy, and Alexandr Shmat'ko. 2011. "Slow-Wave PBG Structures for Terahertz Electronics." Paper presented at the IEEE Crimean International Conference on Microwave and Telecommunication Technology, Sevastopol, Ukraine, September 11–16.
50. Odarenko, Evgeniy, and Alexandr Shmat'ko. 2012. "Photonic Crystal Waveguides in O-Type Electron Devices." Paper presented at the IEEE Crimean International Conference on Microwave and Telecommunication Technology, Sevastopol, Ukraine, September 10–14.
51. Odarenko, Evgeniy, and Alexandr Shmat'ko. 2013. "Enhancement of the Interaction Efficiency in O-Type Electeronical Devices with Photonic Crysral Slow-Wave Systems." Paper presented at the IEEE Crimean International Conference on Microwave and Telecommunication Technology, Sevastopol, Ukraine, September 9–13.
52. Odarenko, Evgeniy, and Alexandr Shmat'ko. 2016. "Novel THz Sources with Profiled Focusing Field and Photonic Crystal Electrodynamic Systems." Paper presented at the IEEE International Conference on Modern Problems of Radio Engineering, Telecommucations, and Computer Science, Lviv-Slavsko, Ukraine, February 23–26.
53. Sashkova, Yulia, *et al*. 2018. "Analysis of Slow Wave Modes in Modified Photonic Crystal Waveguides Using the MPB Package." Paper presented at the

IEEE International Conference on Mathematical Methods in Electromagnetic Theory, Kyiv, Ukraine, July 2–5.
54. Vertiy, Alexey, and Viktor Shestopalov. 1982. “Polarization Effects in Diffraction Radiation Generators – Free Electron Lasers.” *Soviet Physics Doklady* 262(5):1124–27.
55. Vertiy, Alexey, Tsvyk, Alexey, and Viktor Shestopalov. 1985. “Experimental Observation of the Diffraction Radiation Effect in the Millimeter-Wave Range.” *Soviet Physics Doklady* 280(2):343–47.
56. Vertiy, Alexey. 1985. “Study and Applications of Resonant Quasi-Optical Systems for Millimeter Wave Physics.” Doctor of Sciences diss., Kharkiv State University.
57. Vertiy, Alexey, *et al*. 1985. “The Fine Structure of Diffraction Emission in Millimeter Wave Region.” *Radiophysics and Quantum Electronics* 28(10):888–94.
58. Vertiy, Alexey, *et al*. 1987. “Study of Polarization Characteristics of Radiation From a Diffraction Radiation Generator.” *Radiophysics and Quantum Electronics* 30(1):85–92.
59. Lopukhin, Vladimir, and Anatoliy Roshal. 1968. *Electron-Beam Parametric Amplifiers*. Moscow: Sovetskoye Radio.

Reviewed by Prof. Panayiotis Frangos, School of Electrical and Computer Engineering, National Technical University of Athens, Athens, Greece. E-mail: pfrangos@central.ntua.gr. Tel.: +30 210 772 3694. Academic profile: https://www.ece.ntua.gr/en/staff/48.